**Flocculent layers and bacterial mats in the mudstone interbeds of the Primary Lower Gypsum unit (Tertiary Piedmont Basin, NW Italy): archives of palaeoenvironmental changes during the Messinian salinity crisis**

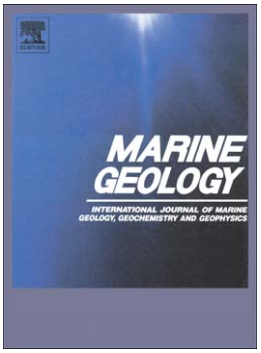


# Flocculent layers and bacterial mats in the mudstone interbeds of the Primary Lower Gypsum Unit (Tertiary Piedmont Basin, NW Italy): Archives of palaeoenvironmental changes during the Messinian salinity crisis

Francesco Dela Pierre, Pierangelo Clari, Marcello Natalicchio, Simona Ferrando, Roberto Giustetto, Francesca Lozar, Stefano Lugli, Vinicio Manzi, Marco Roveri, Donata Violanti

PII: S0025-3227(14)00144-3
DOI: doi: 10.1016/j.margeo.2014.05.010
Reference: MARGO 5109

To appear in: *Marine Geology*

Received date: 1 March 2013
Revised date: 3 April 2014
Accepted date: 19 May 2014

Please cite this article as: Dela Pierre, Francesco, Clari, Pierangelo, Natalicchio, Marcello, Ferrando, Simona, Giustetto, Roberto, Lozar, Francesca, Lugli, Stefano, Manzi, Vinicio, Roveri, Marco, Violanti, Donata, Flocculent layers and bacterial mats in the mudstone interbeds of the Primary Lower Gypsum Unit (Tertiary Piedmont Basin, NW Italy): Archives of palaeoenvironmental changes during the Messinian salinity crisis, *Marine Geology* (2014), doi: 10.1016/j.margeo.2014.05.010

# Flocculent layers and bacterial mats in the mudstone interbeds of the Primary Lower Gypsum Unit (Tertiary Piedmont Basin, NW Italy): archives of palaeoenvironmental changes during the Messinian salinity crisis

Francesco Dela Pierre [1]*, Pierangelo Clari [1], Marcello Natalicchio [1], Simona Ferrando [1], Roberto Giustetto [1], Francesca Lozar [1], Stefano Lugli [2], Vinicio Manzi [3,4], Marco Roveri [3,4], Donata Violanti [1]

*1) Università di Torino, Dipartimento di Scienze della Terra, Via Valperga Caluso 35, 10125, Torino, Italy*

*2) Università di Modena e Reggio Emilia, Dipartimento di Scienze Chimiche e Geologiche, Piazza S. Eufemia 19, 41100, Modena, Italy*

*3) Università di Parma, Dipartimento di Fisica e Scienze della Terra, Parco Area delle Scienze 157/A, 43100, Parma, Italy*

*4) Alpine Laboratory of Palaeomagnetism (ALP), Via Madonna dei Boschi 76, 12016, Peveragno (CN), Italy*

* Corresponding author

E-mail address: francesco.delapierre@unito.it

Phone: +39 0116705198

Fax: +39 0116705339

ABSTRACT

The recognition of peculiar laminated layers atypically rich in a biogenic intrabasinal component in the mudstone intervals from the Messinian (late Miocene) Primary Lower Gypsum unit (5.97-5.60 Ma) of the Piedmont basin (NW Italy) provides information on the palaeoenvironmental evolution at precessional insolation maxima. These cyclic layers consist of irregular alternation of cm-thick grey terrigenous laminae and whitish composite packets; the latter is in turn composed of sub mm-thick wrinkled dolomite-rich laminae that alternate with terrigenous ones. Two types of layers can be distinguished: i) peloidal layers, composed of faecal pellets and irregular diatom-rich aggregates, interpreted as marine snow floccules; ii) filament bearing layers, composed of interwoven filaments up to 150 μm across, corresponding to remains of *Beggiatoa*-like giant sulphide-oxidizing bacteria. By comparison with present-day settings, the peloidal layers are interpreted as flocculent layers, deposited on anoxic sea bottoms, following episodes of phytoplankton bloom in the upper water column. The filament-bearing layers are considered as chemotrophic microbial mats, growing on dysaerobic sea bottoms. The uncommon preservation of both kinds of layers is the result of extensive dolomite precipitation in the shallow subsurface, induced by bacterial sulphate reduction. The laminated layers are the first reported example of a high frequency climate-driven cyclicity in the non-evaporitic portion of the Primary Lower Gypsum unit. Their stacking pattern within the mudstone intervals reflects the gradual increase of the oxygen content of bottom waters during the humid precessional hemicycle, culminating with gypsum deposition at the onset of the arid phase.

*Key words:* marine snow, bacterial mats, Messinian salinity crisis, Primary Lower Gypsum, Piedmont Basin.

## 1. Introduction

The environmental parameters governing evaporite deposition in the Mediterranean region during the Messinian salinity crisis (MSC) are still under discussion. Fundamental aspects of deposition during a high salinity phase involve the depth of deposition and the physico-chemical parameters of the water column and the sea bottom waters (e.g. Rouchy and Caruso, 2006; Ryan, 2009). The correct evaluation of these factors is hindered by the lack of present-day analogues for those Miocene evaporite deposits and by the paucity of biological remains that are preserved in them (e.g. Lugli et al., 2010).

While the original models for the deposition of the Messinian Lower Evaporites suggested a stratigraphic model that applied equally for the shelves, slopes and deep basins (Hsü et al., 1973), more recent work, summarized in the CIESM Consensus Reports (CIESM, 2008) and in an updated synthesis on the MSC evolution (Roveri et al., in press), has proposed that the Messinian stratigraphy of marginal, shallow-water areas is not time equivalent to that of deep basinal areas. According to these detailed stratigraphic reconstructions, the Primary Lower Gypsum unit (PLG; Roveri et al., 2008a) apparently accumulated in shallow peripheral basins of the Mediterranean region during the first stage of the MSC (5.97-5.60 Ma; Manzi et al., 2013). Its deposition took place in an evaporitic basin filled with marine waters but strongly influenced by the input of continental waters (e.g. Longinelli, 1979/1980; Natalicchio et al., 2014). This unit shows a striking lithologic cyclicity, marked by the regular repetition of mudstone/gypsum couplets, reflecting precession-controlled humid/arid climate oscillations (e.g. Krijgsman et al., 1999; 2001; Manzi et al., 2013: Roveri et al., in press). Mudstone layers formed at precession minima (insolation maxima), when river runoff and precipitation exceeded evaporation. Gypsum beds correlate to precession maxima (insolation minima), when evaporation exceeded river runoff and precipitation.

Current environmental reconstructions are mainly based on the study of the gypsum beds, whose different lithofacies (massive, banded and branching selenite) and stacking pattern are thought to reflect oscillations of the brine level and of the saturation conditions during insolation minima characterised by arid climate conditions (e.g. Lu, 2006; Roveri et al., 2008b; Lugli et al., 2010). Moreover, these bottom-grown selenite crystals commonly enclose filamentous remains (the "spaghetti-like structures" of Vai and Ricci Lucchi, 1977) interpreted as fossilized cyanobacteria (e.g. Panieri et al., 2010), thus providing evidence for relatively shallow water depositional conditions. Conversely, the mudstone interbeds, have mostly been neglected. These interbeds contain abundant transported continental fossils (mainly land plant debris and insect remains; Sturani, 1973; Bertini and Martinetto, 2011) and, in some Sicilian examples, filamentous microfossils of unknown origin (Tamajo, 1961). The presence of sparse marine planktic (diatoms) and nektonic (fish) fossil remains (e.g. Landini and Sorbini, 1989; Fourtanier et al., 1991; Carnevale et al., 2008) suggests, however, the local existence of normal marine waters during deposition of the non-evaporitic portion of the PLG unit, even though this interpretation is very controversial. In this regard, the large part of the reconstructions consider that the connection with the Atlantic ocean was still active, albeit restricted (see discussion in Roveri et al., in press). On the other hand, calcareous plankton is virtually absent in these muddy sediments, thus preventing a reliable biostratigraphic and palaeoenvironmental control (e.g. Krijgsman et al., 2001). Also benthic fossils are extremely rare (apart from few exceptions such as the Sorbas basin, where normal marine assemblages have been reported; Saint Martin et al., 2000; Goubert et al., 2001), thus reflecting diffuse anoxic bottom conditions related to a stratified water column (e.g. Sinninghe Damsté et al., 1995; Manzi et al., 2007). As a consequence, no information is available concerning the physico-chemical conditions of the water column during the insolation maxima phase, thus hampering the full understanding of the palaeoenvironmental scenario during the first stage of the MSC.

This paper presents the results of an integrated sedimentological, minero-petrographical and geochemical study focused on peculiar laminated layers within the mudstone interbeds of the PLG

unit of the Piedmont basin (NW Italy). These layers are atypically rich in planktic and benthic microbial fossil remains and provide important clues on the palaeoenvironmental conditions at precessional insolation maxima during the first stage of the crisis.

## 2. Geological and stratigraphic settings

During the Messinian the Piedmont Basin (Fig. 1A) was a wide wedge-top basin, developed upon Alpine, Ligurian and Adria basement units juxtaposed during the mesoalpine collisional event (Mosca et al., 2009; Rossi et al., 2009). The shallow marginal zones of the basin are presently exposed in the southern (Langhe) and northern (Monferrato-Torino Hill) sectors, whereas the depocentral zones are buried below the Pliocene and Quaternary sediments of the Alessandria and Savigliano basins (Figs. 1A, B). The PLG unit was deposited at the basin margins during the first stage of the Messinian salinity crisis (5.97-5.60 Ma) and overlies Tortonian - lower Messinian outer shelf to slope muddy sediments referred to as the Sant'Agata Fossili Marls (Lozar et al., 2010; Dela Pierre et al., 2011; Fig. 1B). It consists of up to 13 precession-related lithologic cycles, composed of alternating mudstone and gypsum layers. Gypsum layers, up to 10 m thick, are made up of massive, banded and branching selenite facies. The latter facies, as elsewhere in the Messinian (Lugli et al., 2010), appears from the sixth bed upwards. On the southern basin margin (where the studied sections are located) this bed actually corresponds to a distinct marker bed (referred to as the Sturani key-bed), which allowed detailed physical-stratigraphic correlations across the basin (Dela Pierre et al., 2011; Fig. 1B). The mudstone beds, up to 2 m thick, are composed of dark grey "euxinic shales" interbedded with thin sandy layers, deposited by fluvial floods sourced by neighbouring continental areas. The macrofossil content consists of transported land plant debris and insects, as well as of sparse fish remains (Sturani, 1973; Gaudant and Cavallo, 2008), including both euryhaline (e.g. *Aphanius crassicaudus*) and stenohaline (e.g *Lepidopus albyi*, *Tavania sturanii*, *Scorpaena* sp.) taxa, that suggested a connection of the basin with the sea. Thin layers of

diatomites were reported between the gypsum layers, but their stratigraphic position is actually poorly constrained (Fourtanier et al., 1991). The diatom assemblage includes open marine taxa (e.g. *Nitzschia marina*, *Thalassiothrix longissima*, *Coscinodiscus* sp.) supporting the input of normal saline waters. A downslope transitional reconstruction of the three lower PLG cycles shows a transition onto laminated mudstones and carbonate-rich beds (Fig. 1B); those carbonate layers were interpreted as the product of lithification of chemotrophic microbial mats dominated by sulphide-oxidizing bacteria (Dela Pierre et al., 2012).

The PLG unit is unconformably overlain by chaotic and resedimented evaporites (Valle Versa Chaotic Complex) which, according to Dela Pierre et al. (2011), can be ascribed to the Resedimented Lower Gypsum unit (Roveri et al., 2008a) deposited during the second MSC stage (5.60-5.55 Ma; Roveri et al., in press) in many Mediterranean basins (Fig. 1B). The basal unconformity corresponds to the Messinian erosional surface and reflects a phase of increased tectonic activity, leading to uplift and erosion of the PLG unit (Dela Pierre et al., 2002, 2007; Natalicchio et al., 2013a). The Messinian succession ends with fluvio-deltaic and lacustrine terrigenous sediments (Cassano Spinola Conglomerates), showing at their base another sharp erosional unconformity, cutting the Messinian erosional surface at the basin margins (Fig. 1B). Deposition of Zanclean marine clays and marls (Argille Azzurre Fm.) marks the end of the salinity crisis at 5.33 Ma (Violanti et al., 2011), as in all the other Mediterranean areas.

## 3. Methods

Field studies of the lithology and sedimentological characteristics of the mudstone intervals of the PLG unit were performed on sections located in the southern margin of the Piedmont basin (Rio Berri, Cascina Merlotti, Pollenzo; see Dela Pierre et al., 2011 for further details). Standard thin sections of carbonate-cemented layers were studied using conventional transmitted, reflected and UV light microscopy. Thin sediment slices cut both parallel and perpendicular to bedding were

obtained from unconsolidated layers and studied under the microscope. Petrographic thin sections were obtained after epoxy impregnation and studied with the same methodology. Scanning electron microscopy (SEM) analyses were performed on 50 slightly etched polished surfaces using a SEM Cambridge Instruments Stereoscan 360 equipped with an energy-dispersive EDS Oxford Instruments Link System microprobe. Carbon-coated thin sections were used for backscattered electron imagery.

X-ray powder diffraction (XRPD) analyses were performed on 11 samples to identify the authigenic carbonate fraction and the main mineralogical components, both qualitatively and quantitatively. Data were collected in the 3-70° 2θ range using an automated Siemens D-5000 diffractometre with a θ/2θ setup in Bragg-Brentano geometry, using graphite monochromatized Cu-Kα radiation and a zero-background flat sample holder, and processed with the Diffrac Plus (2005) evaluation package (EVA 11, 0 0, 3). Quantitative analyses were obtained through model constrained-full pattern analyses with the Rietveld method (GSAS software package; Larson and Von Dreele, 2007, equipped with the EXPGUI graphical user interface; Toby, 2001). Starting structural models for the detected minerals were taken from the American Mineralogist Crystal Structure Database (Downs and Hall-Wallace, 2003).

*In situ* micro-Raman spectra on thin sections were acquired with an integrated micro/macro-Raman LABRAM HRVIS (Horiba Jobin Yvon Instruments) with an excitation line at 632.81 nm produced by HeNe laser at 20 mW of emission power, a Super Notch Plus filter with spectral resolution of 1 $cm^{-1}$, and a grating of 600 grooves/mm. The laser spot size was focussed to 2-5 μm with a 50-100x objectives. 20 to 30 accumulations in the time span of 10 – 30 s were collected for each spectrum. Calibration was performed using the 520.6 $cm^{-1}$ Si band.

Bulk rock C and O stable isotope analyses on the dolomite fraction were performed on 9 samples from both carbonate-rich and unconsolidated layers at the ISO4 Laboratory (Torino) and at the *MARUM* Stable Isotope Laboratory (Bremen). The isotopic ratios are expressed as $\delta^{13}C$ and

$\delta^{18}O$ per mil versus the VPDB standard; the analytical error is ±0.5‰ and ±0.2‰ for $\delta^{13}C$ and $\delta^{18}O$, respectively.

## 4. Results

The distribution of the laminated layers in the studied sections is shown in Fig. 2. Data discussed in this paper derive mainly from the Rio Berri section, in which these layers were recognised for the first time and are excellently exposed. These data are implemented by further non-systematic observations also made from other sections (Cascina Merlotti and Pollenzo).

### *4.1 The Rio Berri section*

In this section a 2 m thick mudstone interval is exposed, directly underlying a 5 m thick gypsum bed (Figs 2, 3). This gypsum layer is in turn overlain by the Sturani-key bed that corresponds to the sixth PLG cycle (Dela Pierre et al., 2011) (Fig. 2). As a consequence, the muddy interval of Rio Berri section can also be referred to cycle PLG 5 (Figs. 2, 3). The base of this cycle (corresponding to the top of underlying gypsum layer) is not exposed at Rio Berri but can be traced from the neighbouring Cascina Merlotti section (Fig. 2).

The bulk of the studied interval is made up of grey mudstone and silty mudstone, commonly very rich in land plant debris. Centimetre-thick coarse- to fine-grained sandstone beds are irregularly interbedded within the mudstone, their grain size increasing upward; these sandy beds show normal grading and, in the upper part, bottom current structures (ripples and crude parallel lamination).

A total of 9 laminated layers that stand, on outcrop, because of their lighter colour, are interbedded with the darker terrigenous sediments (Fig. 3) and their thickness ranges from 1 to 6 cm. The lower 6 layers are irregularly cemented by carbonate (Figs. 3, 4A), whereas the upper 3

ones are mostly unconsolidated (Figs. 3, 4B). Their most remarkable feature is their conspicuous laminated structure (Figs. 4C, D), marked by the alternation of dark grey terrigenous laminae (up to 1 cm-thick) and whitish-coloured packets (up to 2 cm-thick) (Figs. 4E, F). Both these features can be traced along the outcrop for more than ten metres and show a remarkable constant thickness. Terrigenous laminae are composed of siltstone grading upward to mudstone. Their lower boundaries are sharp and can be slightly erosional (Figs. 4E). Whitish composite packets consist of clusters of alternated sub-mm thick wrinkled carbonate-rich laminae (Figs. 4F) and normally graded silt to mud terrigenous ones. Although at a first sight all the layers appear quite similar (apart from the different degree of cementation), two types can be distinguished when whitish packets are observed on sections cut parallel to the bedding: i) peloidal layers and ii) filament-bearing layers.

*4.1.1 Peloidal layers*

These layers (1 to 4, Fig. 3), found in the lower part of the Rio Berri section, show sharp boundaries with the host terrigenous sediments and are irregularly cemented by authigenic carbonate. XRPD data indicate that dolomite, the only carbonate present, is the dominant mineral phase (around 60 to 70 wt% of the whole specimen; Table 1, samples BE1-BE3). Lower values (below 15 wt%) were observed in sample BE4. In addition to dolomite, the presence of quartz was detected together with a variable clay fraction, mainly composed of clinochlore, kaolinite and illite. Both the quartz and clay fractions usually are around 10 wt%, but their quantities tend to increase in those dolomite-poor layers. Muscovite, plagioclase and (occasionally) scarce gypsum complete the mineralogical composition (Table 1).

The dolomite-rich laminae are composed of peloids (more than 90% of total components), sparse silt-sized siliciclastic grains (mostly quartz and muscovite) and carbonaceous fragments. Three different types of peloids can be distinguished, on the basis of their shape, type of boundaries (sharp *vs.* diffuse), internal structure and composition (Fig. 5A):

1) distinct ovoid and subcylindrical faecal pellets, showing definite sharp boundaries, average length of 1-1.5 mm and sub-circular sections up to 500 μm across (Fig. 5B). These peloids are whitish to grey in incident light (Fig. 5A), and strongly opaque in transmitted light (Fig. 5B); furthermore they show a high autofluorescence, suggesting an abundance of organic matter. SEM-EDS analyses showed that these features are composed of clotted dolomicrosparite mixed with clay. Despite their high fluorescence (further supporting the presence of organic matter), Raman data show relatively broad bands, possibly suggesting a low crystallinity degree of the dolomite (Fig. 6). In all spectra, however, the fundamental stretching mode of the $CO_3^{2-}$ ion (1097 $cm^{-1}$) is always recognizable, together with bands at 299 $cm^{-1}$ and 725 $cm^{-1}$, thus unequivocally confirming the ubiquitous presence of dolomite (Fig. 6).

2) Irregular aggregates with diffuse external boundaries. These features are commonly up to 500 μm across, appear whitish in incident light and show a clotted structure in transmitted light resulting from the aggregation of smaller particles (Fig. 5C); their autofluorescence is high (Fig. 5D). SEM-EDS analyses indicate that these aggregates are composed of dolomicrosparite, iron sulphides, silica, silt-sized siliciclastic grains and clay. Raman spectra, although characterised by high fluorescence and relatively broad peaks, further confirm the dolomitic nature of the aggregates.

3) Homogeneous aggregates, up to 500 μm across with sub-rounded to irregular shape and sharp to diffuse external boundaries (Figs. 5C, E). These aggregates appear translucent grey in reflected light and nearly transparent in transmitted light (Figs. 5A, E); their autofluorescence is weak, suggesting that organic matter content might be low (Fig. 5F). SEM-EDS analyses and Raman spectra confirmed the dolomitic composition of these aggregates. Remains of diatoms are frequently recognised within these aggregates. At the optical microscope such remains appear as subcircular (Fig. 7A) or acicular ghosts with a maximum length of 100 μm. Under the SEM, the shapes of elongated and centric diatoms can be recognised (Figs. 7C, E, F). The original silica frustules are replicated by a mosaic of subhedral dolomite crystals, only a few μm across (Fig. 7F), suggesting

that complete dissolution of the opaline skeletons post-dates dolomite precipitation. Despite their poor preservation, some specimens could be identified at the genus level (Bonci, pers. communication, 2012). Elongated forms (Figs. 7C, E) can be ascribed to *Thalassiotrix* sp. and *Thalassionema* sp. whereas the centric ones (Fig. 7F) to *Coscinodiscus* sp. These taxa suggest an open marine environment, with normal salinity conditions. Moreover, well preserved external molds of the genus *Surirella* (Fig. 7D), commonly thriving in freshwater and estuarine environments (e.g. Karthick et al., 2012), were also detected.

Generally, the whitish laminae appear composed of a mixture, which includes all three types of peloids. The amount of the three different peloid types, however, may vary in the different laminae (Fig. 7G), some of them showing predominance of one kind (especially type 3). Finally tiny and commonly corroded planktic foraminifer tests (Fig. 7B) are present in layers BE1, BE2 and BE3 (Fig. 3). Remarkably, the observation of the biogenic material only in the dolomite-rich laminae, but not in the terrigenous ones, suggests that it is not reworked.

*4.1.2 Filament-bearing layers*

Layers 5 to 9 (Fig. 3), found in the upper part of the section, show an average mineralogical composition quite analogous to that described for the peloidal ones (Table 1). XRPD data showed that layers 5 and 6 are irregularly cemented by abundant dolomite (more than 60 to 70 wt%), which once again appears as the exclusive carbonate phase. In the upper, mostly unconsolidated layers (7 to 9, Fig. 3), the amount of dolomite decreases and ranges from 47.7 to 36.5 wt% (Table 1). The clay fraction (clinochlore, kaolinite and illite in various proportions), is around 10 wt% in the lower layers with a moderate increase in the upper ones (i.e. about 18 wt% in sample BE 8; Table 1). The amount of silica (in the form of quartz) does not significantly vary throughout most of the section (between 7 and 13 wt% from BE 5 through BE 8; Table 1), but raises towards the top (almost 24 wt% in BE 9). Muscovite, plagioclase and (scarce) gypsum are also main mineral components.

As stated above, sub-mm thick, normally graded terrigenous laminae, containing large amounts of terrestrial carbonaceous debris, are interbedded with composite dolomite-rich packets (Fig. 4F). However, when the latter is observed in cuts parallel or slightly oblique to bedding, a tangle of curved, interwoven filaments up to 150 μm across and few millimetres long can be observed (Figs 8A, B). These features are mostly parallel to the bedding, though locally some of them apparently penetrate down for a few hundreds of microns into the underlying terrigenous lamina (Fig. 8C). Filaments are mostly white to cream-coloured under incident light (Fig. 8A), strongly opaque in transmitted light (Fig. 8D) and their bright autofluorescence (Fig. 8E) suggests high organic matter content. Some filaments are dark-coloured (light grey or black) (Fig. 8A), due to the presence of scattered framboids of iron sulphide minerals (Fig. 8F). All the filaments show a generally circular outline in cross section, although some specimens appear slightly flattened in the upper unconsolidated layers, possibly due to compaction. No clay and/or siliciclastic grains could be observed within the filaments themselves, although such a fraction was found in the surrounding matrix. SEM-EDS analyses showed that in both cemented and unconsolidated layers the filament bodies are mostly made up of dolomite microcrystals, together with sparse iron sulphide framboids and grains; in the cemented layers, however, dolomite was observed also in the matrix surrounding the filaments. Raman data confirmed the presence of iron sulphides, identified as marcasite and possibly pyrite, in association with dolomite (Fig. 6).

Poorly defined irregular masses, resembling peloids, are present in these layers. Moreover, rare and badly preserved foraminiferal remains were observed in layers BE5 and BE6 (Fig. 3).The initial presence of silica skeletal remains is suggested by some barely recognisable imprints of acicular diatoms.

*4.1.3 Stable isotope data*

Stable isotope data from the Rio Berri section are reported in Table 2. In both peloid- and filament-bearing layers, slightly negative $\delta^{13}C_{dol}$ values, ranging from −4.2 to −1.8 ‰ VPDB were measured; the $\delta^{18}O_{dol}$ values are positive and range from +4.1 to +8.9 ‰ VPDB.

*4.2 Data from other sections*

Laminated layers analogous to those of the Rio Berri were found in other nearby sections (Cascina Merlotti and Pollenzo) (Fig. 2):

*Cascina Merlotti section* - Filament-bearing layers, slightly cemented by carbonate or still unconsolidated, were found in the upper part of the mudstone intervals of cycles PLG 4 (2 layers) Fig. 9A) and PLG 6 (2 layers Figs. 9B, C). Poor outcrop conditions did not allow detailed observations of cycle PLG 5 (the same of Rio Berri).

*Pollenzo section* – An unconsolidated filament-bearing layer was observed below the first local gypsum beds (corresponding to cycles PLG 4) (see Dela Pierre et al., 2011) (Fig. 2). Moreover, two analogous layers were found below the third local bed (the Sturani key-bed), corresponding to cycle PLG 6. The Pollenzo laminated beds are consolidated exclusively by dolomitic cement (40-45 wt%), as for the Rio Berri section (Table 1). In addition to dolomite, considerable consistency between the Rio Berri and Pollenzo sections was further confirmed by the mineralogical composition, the only noteworthy difference being represented by a slightly more conspicuous clay fraction (about 20 wt% as clinochlore + kaolinite + illite) in the latter (Table 1).

## 5. Discussion

The detailed observations made on peloidal and filament-bearing layers allow us to reconstruct the environmental conditions that governed their deposition.

*5.1 Peloidal layers: deposition of marine snow on an anoxic sea bottom*

In the peloidal layers, observed in the lower part of the Rio Berri section (layers BE1 to BE4, Fig. 3), cm-thick terrigenous laminae alternate with packets formed, in turn, by clusters of alternating sub-mm thick grey muddy and whitish dolomite-rich-laminae (Fig. 4E). The main components of the latter are faecal pellets (type 1 peloids) and irregular aggregates that are rich in clay and siliciclastic grains (type 2 peloids) or contain abundant diatom frustules (type 3 peloids). All these features are common constituents of the so-called marine snow (e.g. Alldredge and Silver, 1988), ubiquitously distributed in the water column of present day seas (Herndl et al., 1999). Marine snow is thought to be one of the main vehicles through which organic matter is transported to the sea bottom (e.g. Kiørboe, 2001; Levin, 2003). It is composed of aggregates, commonly larger than 500 μm across, consisting of skeletal remains of planktic biota (diatoms, nannofossils) and clay particles that are entrained in a sticky organic material of algal and/or microbial origin (e.g. Turner, 2002). Marine snow forms during episodes of enhanced primary productivity and phytoplankton bloom in the upper water column (e.g. Alldredge et al., 2002) and originates through the production of zooplankton faecal pellets or, more frequently, through the aggregation of skeletal remains (especially diatoms) and clay particles, floating in the water column (e.g. Thornton, 2002). Its deposition at the sea bottom generates to the so-called flocculent layers (e.g. Graco et al., 2001; Pilskaln and Pike, 2001), that are normally destroyed under oxic conditions by the activity of benthic organisms. Conversely, if seabottom anoxia prevails these layers can be preserved and incorporated in the sedimentary column.

Based on the comparison with present-day settings, the peloidal layers of the PLG unit can be interpreted as Messinian flocculent layers formed by the deposition of marine snow at sea bottom, originating by both zooplankton activity (type 1 peloids) and diatom aggregation following episodes of phytoplankton bloom in the upper water column (type 3 peloids). The origin of type 2

peloids remains still unclear. Such features could represent partially disaggregated faecal pellets, having lost their shape while sinking towards the sea bottom, or composite snow-flakes, formed by aggregation of clay particles and poorly preserved planktic skeletal remains.

*5.2 Filament-bearing layers: fossilized Messinian chemotrophic microbial mats*

In these layers, observed in the upper part of the Rio Berri section (layers BE5 to BE9) as well as in the Pollenzo and Cascina Merlotti sections, the dolomite-rich laminae consist of densely interwoven filaments made up of dolomite microcrystals mixed with silica and, occasionally, with iron sulphide framboids and grains. Remains of planktic biota are much more rare than in the peloidal layers represented only by dubious diatom ghosts, and very rare planktic foraminifers. The size and morphology of the filaments, together with the presence of sulphide minerals suggests that these remains may be related to sulphide-oxidizing giant bacteria (like *Beggiatoa*), as recently suggested for analogous features found in carbonate-rich beds of the neighbouring Pollenzo section (Dela Pierre et al., 2012). These latter beds, however, are slightly older than those described in this work, because they correspond to the deeper water counterpart of the lower three PLG cycles (Fig. 2).

In several present day settings sulphide-oxidizing filamentous bacteria develop in places and times characterised by deposition at the sea bottom, in the form of flocculent layers, of conspicuous amounts of “fresh” organic matter resulting from high productivity rates in the upper water column (e.g. Santa Barbara basin: Soutar and Crill, 1977; Reimers et al. 1990; Black Sea: Pilskan and Pike, 2001; Peru coastal sediments: Graco et al., 2001). Flocculent layers provide a geochemical microenvironment particularly favourable to bacterial sulphate reduction and consequent sulphide production able to sustain sulphide-oxidizing prokaryotes (e.g. Graco et al., 2001). These bacteria are adapted to very low oxygen concentrations; oxygen (and nitrate) is used as an electron acceptor for sulphide oxidation (e.g. Schulz and Jørgensen, 2001). On the basis of the above considerations,

the PLG filament-rich layers are interpreted as the remains of Messinian chemotrophic microbial mats dominated by sulphide-oxidizing giant bacteria. Besides, the presence of filaments sinking down in the underlying terrigenous laminae (Fig. 8C), suggests that these features colonized the sea bottom moving up and down through the sediments, as done by present day *Beggiatoa*, in order to better exploit both the rising hydrogen sulphide flux and the oxygen/nitrate content of waters impinging the bottom (e.g. Suits and Arthur, 2000).

*5.3 Diagenesis of laminated layers*

Petrographic data indicate that the studied layers underwent a complex diagenetic evolution.

*Dolomite precipitation*

The preservation of the delicate structures of peloidal and filament-rich layers is due to the precipitation of a substantial fraction (up to 73.5 wt%) of an authigenic dolomicrosparite cement (Table 1). Lack of compaction suggests that this process was synsedimentary or occurred in a very early diagenetic phase, at very shallow burial depth. Synsedimentary or early diagenetic dolomite was observed in small shallow hypersaline lagoons, produced by degradation of organic matter via bacterial sulphate reduction (Vasconcelos et al., 1995; Vasconcelos and McKenzie, 1997; Warthmann et al., 2000; Wacey et al., 2007). However, the lateral extent and sedimentologic characteristics of the laminated layers and of the encasing sediments (graded terrigenous laminae and beds, presence of open marine biota, absence of any evidence of subaerial exposure) can not be reconciled with a shallow water lagoon environment, but rather suggests that dolomite formation took places in bottom sediments under a relatively deep water column.

Dolomite-cemented layers interbedded to open sea organic-rich terrigenous sediments have actually been reported from both ancient (e.g. Friedman and Murata, 1979; Garrison et al, 1984; Bernoulli and Gunzenhauser, 2001; Dela Pierre et al., 2010; 2012; Natalicchio et al., 2012) and recent deposits (Kelts and McKenzie, 1982; Wefer et al., 1998; Middelburg et al., 1990; Pufahl and

Wefer, 2001; Meister et al., 2006; 2007). In all these examples, dolomite formed at shallow burial depths, governed by different bacterially-mediated reactions: methanogenesis, anaerobic methane oxidation and bacterial sulphate reduction (Bernoulli and Gunzenhauser, 2001; Natalicchio et al., 2012 and reference therein). Since these biological processes regulate the carbon isotope fractionation, stable Carbon isotope signatures of authigenic carbonate minerals are a diagnostic tool for the recognition of the operating bacterial processes (e.g. Kelts and McKenzie, 1982; Pufahl and Wefer, 2001; Meister et al., 2006).

In the studied cases, the $\delta^{13}C_{dol}$ values ($-4.2 < \delta^{13}C_{dol}$ ‰ VPDB$< -1.8$, Table 2) permit to exclude the dominant contribution of both anaerobic methane oxidation (that would result in more negative values), and of methanogenesis (that would result in positive values) (Natalicchio et al., 2012). Conversely, these data might be consistent with degradation of organic matter via bacterial sulphate reduction, even though the slight $^{13}C$ depletion suggests the contribution of other C pools, such as pore water $HCO_3^-$ and/or pre-existing biogenic or detrital carbonates (see below).

Also the interpretation of the positive $\delta^{18}O_{dol}$ values ($+4.1 < \delta^{18}O_{dol}$ ‰ VPDB $< +8.9$) is not straightforward. Such values can be explained assuming the influence of: i) deep diagenetic fluids, originated by dehydratation of smectite clay minerals (e.g. Dählmann and De Lange, 2003) or gas hydrate destabilization (e.g. Pierre and Rouchy, 2004); ii) $^{18}O$ - enriched brines originated by partial evaporation of sea water. The first mechanism can be excluded, since no evidence for the upward rising of deep fluids has been found. Conversely, the involvement of evaporated brines is consistent with the environmental conditions under which the PLG formed. Similar values were reported from Messinian dolostones (Bellanca et al., 2001) that are coeval of the PLG unit, but formed in deeper and more reducing conditions (Manzi et al., 2011).

In the case under study, the brines could either derive from “above”, percolating down into the sedimentary column during the formation of overlying gypsum layer, or from “below”, representing a remnant of the brine from which the underlying gypsum bed formed. In both cases, the brines would be $^{18}O$-enriched but Ca-depleted after the precipitation of gypsum. The first hypothesis is

difficult to justify, as the movement of the brines through the already deposited fine-grained terrigenous sediments would have resulted in the more intense cementation of the topmost layers, which is not the case. Moreover, it contrasts with the very early timing of dolomite precipitation, preventing mechanical compaction in both peloidal and filament-bearing layers. We thus prefer the second hypothesis according to which, dolomite formed at (very) shallow sub-bottom depths in contact with dense residual bottom brines under a stratified water column (Fig. 10A). Dolomite precipitation in still porous sediments was triggered by bacterial sulphate reduction of organic matter that was still highly reactive because oxygen depletion did prevent the efficient remineralization of organic carbon by aerobic bacteria in the water column and in the sediment pore waters. The same process affected the filament-bearing layers (Fig. 10B). In this case, however, bacterial sulphate reduction occurred within buried microbial mats, where the preferential sites for dolomite formation were dead bacterial filaments in which more reactive organic matter was available.

*Silica dissolution*

In the peloidal layers, the imprints of the delicate reliefs of diatom frustules locally recognisable on dolomite crystals (Fig. 7F) further confirm that dolomite precipitation occurred very early, predating the dissolution/precipitation conversion of skeletal opal-A to opal CT, generally considered the early step of silica diagenesis (Reich and Von Rad, 1979; Bernoulli and Gunzenhauser, 2001). Silica diagenesis then proceeded with the complete transformation of opal CT to quartz, the only silica phase recognised in the studied sediments. In filament layers the abundant non-detrital silica fraction suggests the initial presence of silica skeletal remains; the lack of clear imprints on dolomite crystals suggests however that siliceous frustules underwent a nearly complete dissolution before the main phase of dolomite precipitation.

*Absence of calcite microfossils: a diagenetic bias?*

An intriguing characteristic of the studied layers is the scarcity or absence of calcareous plankton remains, that can be ascribed to environmental conditions unfavorable to life of calcite shelled organisms. This explanation is commonly satisfactorily adopted for Mediterranean Messinian sediments, even though still controversial (see Introduction). However, an alternative explanation is that the scarcity of calcite microfossils would result from their dissolution during early diagenetic phases (Figs. 10A, B). This hypothesis is further supported by the total lack of calcite cements and detrital grains in the studied deposits. Two possible factors can have contributed to calcite dissolution: i) Ca-depletion of residual bottom brines, after gypsum precipitation (see above), and ii) increased pore water acidity, related to high hydrogen sulphide fluxes deriving from bacterial sulphate reduction (e.g. Peckmann et al., 2004). Both these factors could have favoured dissolution of skeletal (and detrital) calcite, in turn promoting dolomite formation by supplying $Ca^{2+}$ and $CO_3^{2-}$ ions, thus overcoming $Ca^{2+}$ limitations to dolomite precipitation (e.g. Middelburg et al., 1990). According to this hypothesis, the slightly negative $\delta^{13}C_{dol}$ values would result from the averaging of the "heavier" C pool provided by calcite dissolution and the lighter one deriving from degrading organic matter.

*5.4 Laminated layers: archives of short-term climate changes*

In the MSC sedimentary record, short-term (annual to pluriannual) climate oscillations were inferred from the study of evaporitic deposits (gypsum cumulates and halite) formed at insolation minima (Galeotti et al., 2010; Manzi et al., 2012). These oscillations are recorded by small-scale lithologic cycles, consisting of alternating shaly (more humid climate) and evaporitic (more arid climate) laminae. Conversely, no similar detail has been achieved for the sediments deposited at precessional insolation maxima, that are commonly regarded as entirely composed of flood-transported terrigenous deposits, recording humid climate conditions (e.g. Lugli et al., 2010). The vertical arrangement of the laminated layers described above provides evidence of a more complex

scenario, in which short-term climate changes were superposed to the precessional-driven oscillations (Fig. 11). Comparison with recent and modern varved pelagic and hemipelagic sediments (e.g. Bull and Kemp, 1995; Thunnell et al., 1995; Kemp et al., 2000; Rutten et al., 2000) suggests that the alternation of biogenic and terrigenous laminae observed in whitish packets (Figs 4A, B) records seasonal variations of the quantity and composition of the sediments delivered to the basin floor (red curve, Fig. 11). Terrigenous laminae may reflect the humid season, when precipitation and runoff were greatest; biogenic whitish laminae deposited during the high productive less humid season, following episodes of phytoplankton bloom in the upper photic water layers, fuelled by nutrients influxes (Thunnell et al., 1995). Variations of the biogenic fluxes reaching the sea bottom (e.g. Lange et al., 1997) may justify the compositional changes observed at the single-lamina scale in the peloidal layers (Fig. 7G). The thicker terrigenous laminae interbedded with the whitish packets display a sharp and erosional lower boundary and normal grading (Figs. 4A, B). These sedimentological features suggest that they are the product of rapid depositional events, possibly related to peak fluvial floods.

The analysis of the Rio Berri section shows that, besides the pervasive small scale cyclicity described in the laminated layers, other major rank lithological cycles can be recognised, evidenced by the alternations of terrigenous bedsets and the laminated layers themselves (Fig. 11). Although the periodicity of this cyclicity is not clear yet, we propose that it was driven by longer term (plurisecular to millenary?) climate oscillations responsible for the deposition of terrigenous bedsets during phases of enhanced river runoff and of laminated layers during phases of lower terrigenous input (black curve, Fig. 11).

### 5.5 *Environmental evolution at precessional insolation maxima*

The results presented in previous sections allow us to discuss the environmental changes that occurred at precessional insolation maxima, when the hydrological budget of the basin(s) was

maintained at positive values by predominant fresh water inflows that exceeded evaporation (e.g. Krijgsman and Meijer, 2008; Topper and Meijer, 2013). An ideal facies cycle, starting with peloidal layers, continuing with filament-bearing ones and culminating with the gypsum bed (Fig. 11) can be defined.

The absence of filaments in peloidal layers and the rarity of peloidal remains in filament-bearing ones is in apparent contrast with what observed in present day environments, in which the development of chemotrophic microbial mats is intimately linked to the deposition of flocculent layers (e.g. Graco et al., 2001). In our examples, conversely, peloids and filaments characterise clearly separated layers (Fig. 11). This apparent discrepancy could be explained by an overall increase of the oxygen content of bottom waters, going from peloidal to filament-bearing layers (and eventually to the gypsum). The preservation of marine snow textures in the peloidal layers and the absence of sulphide-oxidizer remains could reflect prolonged persistence of anoxic conditions in the lower water column and in the bottom waters (Fig. 10A). Conversely, sulphide oxidizing microbial mats thrived under dysaerobic bottom conditions (Fig. 10B); oxygen concentration was too scarce to sustain macro- and microinvertebrate benthic associations but sufficient to guarantee respiration of *Beggiatoa*-like bacteria (capable of using, besides oxygen, nitrate ions from sea water for sulphide oxidation; Schultz and Jørgensen 2001; Mussmann et al. 2003).

The oxygen content at the sea bottom and in the water column in closed or semi-enclosed basins is driven by the interaction of several factors, including fluvial activity and fresh water inflows, nutrient influxes, current circulation patterns and depth changes (e.g. Tyson and Pearson, 1991). In the case under study, oxygen depletion and stagnant bottom conditions during deposition of peloidal layers reflect severe density stratification of the water column, in turn resulting from the presence of dense bottom brines (positive $\delta^{18}O$ values of dolomite cement), overlain by less saline superficial waters with high primary productivity (high riverine runoff) (see Fig. 10A). The presence of brackish (e.g. *Surirella* sp.) and open marine (*Thalassiotrix*, *Coscinodiscus* sp.) diatoms and sparse planktic foraminifers strongly suggests that salinity of superficial waters was highly

variable but, at least in some parts, reached values close to that of sea water, suitable for the life requirement of calcareous and siliceous planktic biota. An important consequence is that the basin was connected with a marine water body from which these taxa could migrate. In addition, although the depth of the basin can not be confidently estimated, diffuse bottom anoxia suggests that it was enough to be beyond the reach of the effect of seasonal wind-driven turbulence (Tyson and Pearson, 1991).

The shift towards more oxygenated bottom condition is testified by the appearance of filament-bearing layers. This renovated condition might be the result of different processes, acting in close interaction:

1) cooling of superficial waters at the transition to precessional insolation minima. The reduction of the density gradients between superficial waters and bottom brines resulted in a less stratified water column and in the slight oxygenation of the bottom water (Filippelli et al., 2003; Flores et al., 2005). River runoff and nutrient influxes were still enough for deposition and bacterial degradation of organic-rich sediments and thus for the generation of hydrogen sulphide fluxes necessary for the life of *Beggiatoa*-like prokaryotes;

2) shallowing of the basin, making vertical mixing of the water column more efficient (Fig. 10B). This is supported by the increase of grain size of terrigenous sediments encasing the filament-bearing layers, that suggests an overall regressive trend. However, the bottom of the basin did not reach necessarily the photic zone, since sulphide-oxidizing bacteria are not phototrophic organisms and do not necessitate light (e.g. Bailey et al., 2009).

The onset of gypsum deposition could reflect a further increase of the oxygen content of bottom waters, resulting from the decrease of fluvial activity and nutrient influxes (favouring the reduction of salinity gradients and lowering primary productivity) and from further shallowing of the basin (favoring mixing of the water column); low oxygen content would be in fact a limiting factor for gypsum formation and preservation, because intense bacterial sulphate reduction lowers sulphate concentration and leads to undersaturation with respect to gypsum (Babel, 2007; De Lange and

Krijgsman, 2010). However, preliminary studies (Natalicchio et al., 2013b) show that the solid content of some Piedmont bottom-grown selenite crystals is actually very similar to that of the studied laminated layers, consisting of brackish and open marine diatoms and marine snow flakes. This suggests that riverine runoff, nutrient influxes and deposition of organic-rich laminae continued during gypsum deposition. The influence of fresh water inflows is further supported by fluid inclusion data from gypsum crystals, that point to salinities lower than that of sea waters (Nataliccho et al., 2014). Moreover, the gypsum crystals contain a network of interwoven filaments whose size and shape (commonly outlined by tiny iron sulphide grains) is similar to the features observed in filament-bearing layers. On this basis, we suspect that these "spaghetti-like structures" could represent remains of sulphide-oxidizing bacteria (and not cyanobacteria), as recently suggested by Schopf et al. (2012). These observations, along with the surprisingly low salinities values recorded in Piedmont selenites, raise the question whether, besides evaporation of sea water, other processes such as bacterially-mediated sulphur cycling reactions, fuelled by organic matter degradation, may have contributed to widespread precipitation of gypsum during the first stage of the MSC.



**6. Conclusions**

1) The mudstone interbeds of the Piedmont PLG unit are are not exclusively composed of terrigenous sediments but enclose peculiar laminated beds that contain a remarkable intrabasinal biogenic component, providing information on the palaeoenvironmental conditions at precessional insolation maxima. The presence of open marine planktic biota (diatoms and rare foraminifers) confirms that the northernmost Mediterranean subbasin was connected with a marine water body. The water column was strongly influenced by continental water via river runoff; the resulting input of nutrients promoted phytoplankton blooms, the deposition of marine snow and the development of chemotrophic microbial mats on anoxic/dysaerobic sea bottoms.

2) The exceptional preservation of these features is the result of complex biogeochemical cycles (involving both sulphate reduction and sulphide oxidation) taking place in organic-rich sediments. Bacterial degradation of organic matter in anoxic pore waters induced the early precipitation of dolomite in the very shallow subsurface. The scarcity of calcite skeletal remains could be a diagenetic bias and not necessarily the consequence of inhospitable environmental conditions in the water column.

3) The laminated layers are an archive of short-term climate changes superposed to the precession-driven cyclicity. The alternation of biogenic and terrigenous laminae provides evidence that at precessional insolation maxima the climate was not permanently wet, but oscillated between more and less humid conditions. Moreover, the stacking pattern of the laminated layers permits to define an ideal facies cycle within the "humid" precessional hemicycle, starting with peloidal layers, continuing with filament layers and culminating with gypsum. This vertical evolution would reflect the gradual increase of the oxygen content of bottom waters, related to the progressive weakening of the stratification of the water column.

Further studies, extended to other Mediterranean PLG sections, are needed, especially devoted to i) the definition of the periodicity of short-term climate changes in the mudstone semicouplets, which may help to constrain the relative time duration of the "humid" and "arid" precessional hemicycles, and ii) the comparison of the palaeobiological content of the non evaporitic sediments with that trapped in the gypsum layers, in order to unambiguously define the depositional environment of the PLG unit and the cyclic variation of the physico-chemical parameters of the water body during the first stage of the MSC.

Acknowledgements

Research funded with MIUR grant (Prin 2008, National coordinator M. Roveri), PROactive Management of GEOlogical Heritage in the PIEMONTE Region project (co-founded by the University of Turin - Compagnia di San Paolo Bank, Project Id: ORTO11Y7HR, P.I. M. Giardino),

and University of Torino 2012 funds (ex 60% grant to F. Dela Pierre). Raman analytical facilities were provided by the Interdepartmental Center "G. Scansetti" for Studies on Asbestos and Other Toxic Particulates and by the Compagnia di San Paolo, Torino, Italy. The authors wish to thank M.C. Bonci (Genova University) for identification of diatoms, S. Cavagna and E. Costa (Torino University) for their help with SEM analyses and thin section preparation, and G. Carnevale for discussion. G.J. de Lange, B.C. Schreiber and an anonymous reviewer are thanked for helpful comments and suggestions that greatly improved this manuscript.

**References**

Alldredge, A.L., Silver, M.W., 1988. Direct observations of the mass flocculation of diatom blooms: characteristics, settling velocities, and formation of diatom aggregates. Limnology and Oceanography 20, 41-82.

Alldredge, A.L., Cowles, T.J., MacIntyre, S., Rines, J.E.B., Donaghay, P.L., Greenlaw, C.F., Holliday, D.V., Dekshenieks, M.M., Sullivan, J.M., Zaneveld, J.R., 2002. Occurrence and mechanisms of formation of a dramatic thin layer of marine snow in a shallow Pacific fjord. Marine Ecology Progress Series 233, 1-12.

Bąbel, M., 2007. Depositional environments of a salina type evaporite basin recorded in the Badenian gypsum facies in northern Carpathian Foredeep, In: Schreiber, B. C., Lugli, S., Bąbel, M. (Eds), Evaporites Through Space and Time. Geological Society of London, Special Publication 285, 107-142.

Bailey, J.V., Orphan, V.J., Joye, S.B, Corsetti, F., 2009. Chemotrophic microbial mats and their potential for preservation in the rock record. Astrobiology 9 (Special Issue), 1-17.

Bellanca, A., Caruso, A., Ferruzza, G., Neri, R., Rouchy, J.M., Sprovieri, M., and Blanc-Valleron, M.M., 2001. Sedimentary record of the transition from marine to hypersaline conditions in the Messinian Tripoli Formation in the marginal areas of the Sicilian Basin. Sedimentary Geology 140, 87-106.

Bernoulli, D., Gunzenhauser, B., 2001. A dolomitized diatomite in an Oligocene - Miocene deep-sea fan, Gonfolite Lombarda Group, Northern Italy. Sedimentary Geology 139, 71-91.

Bertini, A., Martinetto, E., 2011. Reconstruction of vegetation transects for the Messinian-Piacenzian of Italy by means of comparative analysis of pollen, leaf and carpological records. Palaeogeography, Palaeoclimatology, Palaeoecology 304, 230-246.

Bigi, G., Cosentino, D., Parotto, M., Sartori, R., Scandone, P., 1990. Structural Model of Italy: Geodinamic Project: Consiglio Nazionale delle Ricerche, S.EL.CA, scale 1:500,000, sheet 1.

Bull, D., Kemp, A.E.S., 1995. Composition and origins of laminae in Late Quaternary and Holocene sediments from the Santa Barbara Basin, In: Baldauf, J.C., Lyle, M. (Eds.), Proceeding of the Ocean drilling Program, Scientific Results 146, 77-87.

Carnevale, G., Caputo, D., Landini, W., 2008. A leerfish (Teostei, Carangidae) from the Messinian evaporite succession of the Vena del Gesso basin (Romagna Apennines, Italy): Palaeogeographical and palaeoecological implications. Bolletino della Società Paleontologica Italiana 47, 169-176.

CIESM, 2008. The Messinian Salinity Crisis from mega-deposits to microbiology – A consensus report. CIESM Workshop Monographs N° 33, F. Briand Eds, Monaco, pp.168.

Dählmann, A., De Lange, G. J., 2003. Fluid-sediment interactions at Eastern Mediterranean mud volcanoes: a stable isotope study from ODP Leg 160. Earth and Planetary Science Letters 212, 377-391.

De Lange, G. J., Krijgsman, W., 2010. Messinian salinity crisis: a novel unifying shallow gypsum/deep dolomite formation mechanism. Marine Geology 275, 273-277.

Dela Pierre, F., Clari, P., Cavagna, S., Bicchi, E., 2002. The Parona chaotic complex: a puzzling record of the Messinian (Late Miocene) events in Monferrato (NW Italy). Sedimentary Geology 152, 289-311.

Dela Pierre, F., Festa, A., Irace, A., 2007. Interaction of tectonic, sedimentary and diapiric processes in the origin of chaotic sediments: an example from the Messinian of Torino Hill (Tertiary Piedmont Basin, northwestern Italy). Geological Society of America Bulletin 119, 1107-1119.

Dela Pierre, F., Martire, L., Natalicchio, M., Clari, P., Petrea, C., 2010. Authigenic carbonates in the upper Miocene sediments of the Tertiary Piedmont Basin (NW Italy): vestiges of an ancient gas hydrate stability zone? Geological Society of America Bulletin 122, 994-1010.

Dela Pierre, F., Bernardi, E., Cavagna, S., Clari, P., Gennari, R., Irace, A., Lozar, F., Lugli, S., Manzi, V., Natalicchio, M., Roveri, M., Violanti, D., 2011. The record of the Messinian salinity crisis in the Tertiary Piedmont Basin (NW Italy): The Alba section revisited. Palaeogeography, Palaeoclimatology, Palaeoecology 310, 238-255.

Dela Pierre, F., Clari, P., Bernardi, E., Natalicchio, M., Costa, E., Cavagna, S., Lozar, F., Lugli, S., Manzi, V., Roveri, M., Violanti, D., 2012. Messinian carbonate-rich beds of the Tertiary Piedmont Basin (NW Italy): microbially-mediated products straddling the onset of the salinity crisis. Palaeogeography, Palaeoclimatology, Palaeoecology 344-345, 78-93

Downs, R.T., Hall-Wallace, M., 2003. The American Mineralogist Crystal Structure Database. American Mineralogist 88, 247-250.

Filippelli, G.M., Sierro, F.J., Flores, J.A., Vàzquez, A., Utrilla, R., Pérez-Folgado, M., Latimer, J.C., 2003. A sediment-nutrient oxygen feedback responsible for productivity variations in Late Miocene sapropel sequences of the Western Mediterranean. Palaeogeography Palaeoclimatology Palaeoecology 190, 335-348.

Flores, J.A., Sierro, F.J., Filippelli, G.M., Barcena, M.A., Perez-Folgado, M., Vàzquez, A., Utrilla, R., 2005. Surface water dynamics and phytoplankton communities during deposition of cyclic late Messinian sapropel sequences in the western Mediterranean. Marine Micropaleontology 56, 50-79.

Fourtanier, E., Gaudant, J., Cavallo, O., 1991. La diatomite de Castagnito (Piémont): une nouvelle preuve de l'existence d'oscillations modérées du niveau marine pendant le Messinien évaporitique. Bollettino della Società Paleontologica Italiana 30, 79-95.

Friedman, I., Murata, K. J. 1979. Origin of dolomite in Miocene Monterey Shale and related formations in the Temblor Range, California. Geochimica et Cosmochimica Acta 43, 1357-1365.

Galeotti, S., von der Heydt, A., Huber, M., Bice, D., Dijkstra, H., Jilbert, T., Lanci, L., Reichart, GJ, 2010. Evidence for active El Niño Southern Oscillation variability in the Late Miocene greenhouse climate. Geology 38, 419-422.

Garrison, R.E., Kastner, M., and Zenger, D.H., 1984. Dolomites of the Monterey Formation and Other Organic-Rich Units. Soc. Econ. Paleontol. Mineral., Pacific Sect. 41, 215 pp.

Gaudant, J., Cavallo, O., 2008. The Tortonian-Messinian fish faunas of Piedmont (Italy) and the Adriatic trough: a synthesis dedicated to the memory of Carlo Sturani (1938-1975). Bollettino della Società Paleontologica Italiana 47, 177-189.

Goubert, E., Néraudeau, D., Rouchy, J.M., Lacour, D., 2001. Foraminiferal record of environmental changes: Messinian of the Los Yesos area (Sorbas Basin, SE Spain). Palaeogeography, Palaeoclimatology, Palaeoecology 175, 61-78.

Graco, M., Farìas, L., Molina, V., Guitiérrez, D., Nielsen, L.P. 2001. Massive developments of microbial mats following phytoplankton blooms in a naturally eutrophic bay: implications for nitrogen cycling. Limnology and Oceanography 46, 821-832.

Herndl, G.J., Arrietta, J.M., Stoderegger, K., 1999. Interaction between specific hydrological and microbial activity leading to extensive mucilage formation in the Northern Adriatic sea. Annali Istituto Superiore Sanità 35, 405-409.

Hsü, K.J., Cita, M.B., Ryan, W.B.F., 1973. The origin of the Mediterranean evaporites, In: Ryan, W.B.F., Hsü, K.J., et al. (Eds.), Initial Report of Deep Sea Drilling Program 13. U.S. Government Printing Office, Washington DC, pp. 1203-1231.

Karthick, B., Hamilton, P.B., Kociolek J.P., 2012. Taxonomy and biogeography of some *Surirella* Turpin (Bacillariophyceae) taxa from Peninsular India. Nova Hedwigia 141, 81-116.

Kelts, K., McKenzie, J.A, 1982. Diagenetic dolomite formation in Quaternary anoxic diatomaceous muds of Deep Sea Drilling Project Leg 64, Gulf of California, In Curray, J.R., Moore, D.G., et al. (Eds.), Initial reports of the Deep Sea Drilling Project 64. U.S. Government Printing Office, Washington, DC, pp. 553-569.

Kemp, E.S., Pike, J., Pearce, R.B., Lange, C.B., 2000. The "Fall dump" – a new perspective on the role of a "shade flora" in the annual cycle of diatom production and export flux. Deep-Sea Research II 47, 2129-2154.

Kiørboe, T. , 2001. Formation and fate of marine snow: small-scale processes with large-scale implication. Scientia Marina 65, 57-71.

Krijgsman, W., Hilgen, F.J., Raffi, I., Sierro, F.J., Wilson, D.S., 1999. Chronology, causes and progression of the Messinian salinity crisis. Nature 400, 652-655.

Krijgsman, W., Fortuin, A.R., Hilgen, F.J., Roep, T.B., Sierro, F. J., 2001. Astrochronology for the Messinian Sorbas Basin (SE Spain) and orbital (precessional) forcing for evaporite cyclicity. Sedimentary Geology 140, 43-60.

Krijgsman, W., Meijer, P.T., 2008. Depositional environments of the Mediterranean "Lower Evaporites" of the Messinian salinity crisis: constraints from quantitative analyses. Marine Geology 253, 73-81.

Landini, W., Sorbini, L., 1989. Ichthyofauna of the evaporitic Messinian in the Romagna and Marche regions. Bollettino della Società Paleontologica Italiana 28, 287-293.

Lange, C.B.,Weinheimer, A.L., Reid, F.M.H., Thunnel, R.C., 1997. Sedimentation patterns of diatoms, radiolarians, and silicoflagellates in Santa Barbara basin, California. CalCOFI Report 38, 161-170.

Larson, A.C., Von Dreele, R.B. 2007. GSAS – General Structure Analysis System. Los Alamos National Laboratory Report No. LAUR 86-748.

Levin, L.A. 2003. Oxygen minimum zone and benthos: adaption and community response to hypoxia. Oceanography and Marine Biology: an annual review 41, 1-45.

Longinelli, A., 1979/1980. Isotope geochemistry of some Messinian evaporites: Paleoenvironmental implications. Palaeogeography, Palaeoclimatology, Palaeoecology 29, 95-123.

Lozar, F., Violanti, D., Dela Pierre, F., Bernardi, E., Cavagna, S., Clari P., Irace, A., Martinetto, E., Trenkwalder, S., 2010. Calcareous nannofossils and foraminifers herald the Messinian salinity crisis: the Pollenzo section (Alba, Cuneo; NW Italy). Geobios 43, 21-32.

Lu, F.H., 2006. Lithofacies and water-body record of Messinian evaporites in Nijar basin, SE Spain. Sedimentary Geology 188-189, 115-130.

Lugli, S., Manzi, V., Roveri, M., Schreiber, B.C., 2010. The Primary Lower Gypsum in the Mediterranean: a new facies interpretation for the first stage of the Messinian salinity crisis. Palaeogeography, Palaeoclimatology, Palaeoecology 297, 83-99.

Manzi, V., Roveri, M., Gennari, R., Bertini, A., Biffi, U., Giunta, S., Iaccarino, S., Lanci, L., Lugli, S., Negri, A., Riva, A., Rossi, M.E., Taviani, M., 2007. The deep-water counterpart of the Messinian Lower Evaporites in the Apennine foredeep: the Fanantello section (Northern Apennines, Italy). Palaeogeography, Palaeoclimatology, Palaeoecology 251, 470-499.

Manzi, V., Lugli, S., Roveri, M., Schreiber, B.C., Gennari, R., 2011. The Messinian "Calcare di Base" (Sicily, Italy) revisited. Geological Society of America Bulletin 123, 347-370.

Manzi, V., Gennari, R., Lugli, S., Roveri, N., Scafetta, N., Schreiber, B.C., 2012. High-frequency cyclicity in the Mediterranean Messinian evaporites: evidence for solar-lunar climate forcing. Journal of Sedimentary Research 82, 991-1005.

Manzi, V., Gennari, R., Hilgen, F., Krijgsman, W., Lugli, S., Roveri, M., Sierro, F.J., 2013. Age refinement of the Messinian salinity crisis onset in the Mediterranean. Terra Nova 25, 315-322.

Meister, P., McKenzie, J.A., Warthmann, R., and Vasconcelos, C., 2006. Mineralogy and petrography of diagenetic dolomite, Peru margin, ODP Leg 201. In Jørgensen, B.B., D'Hondt, S.L., and Miller, D.J. (Eds.), Proc. ODP, Sci. Results 201 pp.

Meister, P., McKenzie, J.A., Vasconcelos, C., Bernasconi, S., Frank, M., Gutjahr, M., Schrag, D.P., 2007. Dolomite formation in the dynamic deep biosphere, results from the Peru Margin, OPD Leg 201. Sedimentology 54, 1007-1032.

Middelburg, J.J., de Lange, G.J., Kreulen, R., 1990. Dolomite formation in anoxic sediments of Kau Bay, Indonesia. Geology 18, 399-402.

Mosca, P., Polino, R., Rogledi, S., Rossi, M., 2009. New data for the kinematic interpretation of the Alps–Apennines junction (Northwestern Italy). International Journal of Earth Sciences 99, 833-429.

Mussman, M., Schulz, H.N., Strotmann, B., Kyær, T., Nielsen, L.P., Rossellò-Mora, R.A., Amann, R.I., Jørgensen, B.B., 2003. Phylogeny and distribution of nitrate-storing *Beggiatoa* spp. in coastal marine sediments. Environmental Microbiology 5, 523-533.

Natalicchio, M., Birgel, D., Dela Pierre, F., Martire, L., Clari, P., Spötl, C., Peckmann, J., 2012. Polyphasic carbonate precipitation in the shallow subsurface: insights from microbially-formed authigenic carbonate beds in upper Miocene sediments of the Tertiary Piedmont Basin (NW Italy). Palaeogeography, Palaeoclimatology, Palaeoecology 329-330, 158-172.

Natalicchio, M., Dela Pierre, F., Clari, P., Birgel, D., Cavagna, S., Martire, L., Peckmann, J., 2013a. Hydrocarbon seepage during the Messinian salinity. Palaeogeography, Palaeoclimatology, Palaeoecology 390, 68-80.

Natalicchio, M., Dela Pierre, F., Clari, P., 2013b. New palaeonvironmental implications for the Messinian salinity crisis: insights from the Primary Lower Gypsum Unit of the Piedmont Basin (NW Italy). RCMNS 14th Congress, Istanbul (Turkey) 8-12 September 2013, Book of Abstracts, pp. 59.

Natalicchio, M., Dela Pierre, F., Lugli, S., Lowenstein, T.K, Feiner, S. J., Ferrando, S., Manzi, V., Roveri, M., Clari, P., 2014. Did late Miocene (Messinian) gypsum precipitate from evaporated marine brines? Insight from the Piedmont Basin (Italy). Geology 42, 179-182.

Panieri, G., Lugli, S., Manzi, V., Roveri, M., Schreiber, C.B., Palinska, K.A., 2010. Ribosomal RNA gene fragments from fossilized cyanobacteria identified in primary gypsum from the late Miocene, Italy. Geobiology 8, 101-111.

Peckmann, J., Thiel, V., Reitner, J., Taviani, M., Aharon, P., Michaelis,W., 2004. A microbial mat of a large sulfur bacterium preserved in a Miocene methane-seep limestones. Geomicrobiology Journal 21, 247-255.

Pierre, C., Rouchy, J.M., 2004. Isotopic compositions of diagenetic dolomites in the Tortonian marls of the Western Mediterranean margins: evidence of past gas hydrate formation and dissociation. Chemical Geology 205, 469-484.

Pilskaln, C.H., Pike, J., 2001. Formation of Holocene sedimentary laminae in the Black Sea and the role of the benthic flocculent layer. Paleoceanography 16, 1-19.

Pufahl, P. K, Wefer, G., 2001. Data report: Petrographic, cathodoluminescent, and compositional characteristics of organogenic dolomites from the southwest African margin, In: Wefer, G; Berger, WH; Richter, C (Eds.), Proceedings of the Ocean Drilling Program, Scientific Results, College Station, TX (Ocean Drilling Program) 175, 1-17.

Reich, V., Von Rad, U., 1979. Silica diagenesis in the Atlantic Ocean: diagenetic potential and transformation, In: Talwani, M., Hay, W., Ryan, W.B.F. (Eds.), Deep drilling results in the Atlantic Ocean: continental margins and paleoenvironments. American Geophysical Union Maurice Ewing Series 3, 315-341.

Reimers, C.E., Lange, C.B., Tabak, M., Bernhard, J.M., 1990. Seasonal spillover and varve formation in the Santa Barbara Basin, California. Limnol. Oceanogr. 35, 1577-1585.

Rossi, M., Mosca, P., Polino, R., Biffi, U., 2009. New outcrop and subsurface data in the Tertiary Piedmont Basin (NW Italy): unconformity bounded stratigraphic units and their relationships with basin modification phases. Rivista Italiana di Paleontologia e Stratigrafia 115, 305-335.

Rouchy, J. M., Caruso, A., 2006. The Messinian Salinity Crisis in the Mediterranean basin: a reassessment of data and an integrated scenario. Sedimentary Geology 188-189, 35-67.

Roveri, M., Lugli, S., Manzi, V., Schreiber, B.C., 2008a. The Messinian Sicilian stratigraphy revisited: new insights for the Messinian Salinity Crisis. Terra Nova 20, 483-488.

Roveri, M., Lugli, S., Manzi, V., Schreiber, B.C., 2008b. The Messinian salinity crisis: a sequence-stratigraphic approach. In: Amorosi, A., Haq, B.U., Sabato, L. (Eds.), Advances in application of sequence stratigraphy in Italy. Geo Acta, Special Publication 1, 169-190
.

Roveri, M., Flecker, R, Krijgsman, W., Lofi, J., Lugli, S., Manzi, V., Sierro, F. J., Bertini, A., Camerlenghi, A., de Lange, G.J., Govers, R., Hilgen, F.J., Hübscher, C., Meijer, P.T., Stoica, M., in press. The Messinian Salinity Crisis: Past and future of a great challenge for marine sciences. Marine Geology doi: 10.1016/j.margeo.2014.02.00

Rutten, A., de Lange, G.J., Ziveri, P., Thomson, J., van Santwoort, P.J.M., Colley, S., Corselli, C., 2000. Recent terrestrial and carbonate fluxes in the pelagic eastern Mediterranean; a comparison between sediment trap and surface sediment. Palaeogeography, Palaeoclimatology, Palaeoecology 158, 197-213.

Ryan, W.B.F., 2009. Decoding the Messinian salinity crisis. Sedimentology 56, 95-136.

Saint Martin, J.P., Néraudeau, D., Lauriat-Age, A., Goubert, E., Secrétan, S., Babinot, J.F., Boukli-Hacene, S., Pouyet, S., Lacour, D., Pestrea, S., Conesa, G., 2000. La faune interstratifiée dans le gypses Messiniens de Los Yesos (Bassin de Sorbas, SE Espagne): implications. Geobios 33, 637-649.

Schopf , W.J., Farmer, J.D., Foster, I.S., Kudryavtsev, A.B., Gallardo, V.A., Espinoza, C., 2012. Gypsum-permineralized microfossils and their relevance for the search for life on Mars. Astrobiology 12, 619-633.

Schulz, H.N., Jørgensen, B.B., 2001. Big bacteria. Annuual Review of Microbiology. 55, 105-37.

Sinninghe Damsté, J.S., Frewin, N.L., Keely, B.J., Maxwell, J.R, 1995. Product distributions from chemical degradation of kerogens from a marl from a Miocene evaporitic sequence (Vena del Gesso, N. Italy). Organic Geochemistry 23, 471-483.

Soutar, A., Crill, P.A., 1977. Sedimentation and climatic patterns in the Santa Barbara Basin during the 19th and 20th centuries. Geological Society of America Bulletin 88, 1161-1172.

Sturani, C., 1973. A fossil eel (*Anguilla* sp.) from the Messinian of Alba (Tertiary Piedmont Basin). Palaeoenvironmental and palaeogeographic implications, In: Messinian events in the Mediterranean. K. Nederl. Akad. Wetensch., Amsterdam, pp. 243-255.

Suits, N.S., Arthur, A.A., 2000. Bacterial production of anomalously high dissolved sulfate concentrations in Peru slope sediments: steady-state sulfur oxidation, or transient response to end of El Niño? Deep Sea Research I 47, 1829-1853.

Tamajo, E., 1961. Probabili tracce di vita in livelli ritenuti azoici della formazione zolfifera siciliana. Rivista Mineraria Siciliana 67, 3-11.

Thornton, D.C., 2002. Diatom aggregation in the sea: mechanisms and ecological implications. European Journal of Phycology 37, 149-161.

Thunnell, R.C., Tappa, E., Anderson, D.M., 1995. Sediment fluxes and varve formation in Santa Barbara Basin, offshore California. Geology 23, 1083-1086.

Toby, 2001. EXPGUI, a graphical user interface for GSAS, Journal of Applied Crystallography 34, 210-213.

Topper, R.P.M., Meijer, P.Th., 2013. A modelling perspective on spatial and temporal variations in Messinian evaporite deposits. Marine Geology 336, 44-60.

Turner, J. T., 2002. Zooplankton fecal pellets, marine snow and sinking phytoplankton blooms. Aquatic Microbial Ecology 27, 57-102.

Tyson, R.V., Pearson, T.H., 1991. Modern and ancient continental shelf anoxia: an overview. Geological Society Special Publication 58, 1-24.

Vai, G.B., Ricci Lucchi, F., 1977. Algal crusts, autochtonous and clastic gypsum in a cannibalistic evaporite basin; a case history from the Messinian of Northern Apennine. Sedimentology 24, 211-244.

Vasconcelos, C., McKenzie, J.A., Bernasconi, S., Grujic, D., Tien, A.J., 1995. Microbial mediation as a possible mechanism for natural dolomite formation at low temperature. Nature 377, 220-222

Vasconcelos, C., McKenzie, J.A., 1997. Microbial mediation of modern dolomite precipitation and diagenesis under anoxic conditions (Lagoa Vermelha, Rio de Janeiro, Brazil). Journal of Sedimentary Research 67, 378-390.

Violanti, D., Dela Pierre, F., Trenkwalder, S., Lozar, F., Clari, P., Irace, A., d'Atri, A., 2011. Biostratigraphic and palaeoenvironmental analyses of the Messinian/Zanclean boundary and Zanclean succession in the Moncucco quarry (Piedmont, northwestern Italy). Bulletin Société Géologique de France, 182, 149-162.

Wacey, D., Wright, D.T., Boyce, A.J., 2007. A stable isotope study of microbial dolomite formation in the Coorong Region, South Australia. Chemical Geology 244, 155-174.

Warthmann, R., van Lith, Y, Vasconcelos, C., McKenzie , J.A., Karpoff, A.M., 2000. Bacterially induced dolomite precipitation in anoxic culture experiments. Geology 28, 1091-1094.

Wefer, G., Berger, W.H., Richter, C., and Shipboard Scientific Party, 1998. Facies patterns and authigenic minerals of upwelling deposits off southwest Africa, In Wefer, G., Berger, W.H., Richter, C., et al. (Eds.), Proc. ODP, Init Reports 175: College Station, TX (Ocean Drilling Program), 487-504.

**Figure Captions**

Fig. 1

A) Structural sketch map of NW Italy. TH: Torino Hill; MO: Monferrato, AM: Alto Monferrato; BG: Borbera Grue; VVL: Villalvernia-Varzi Line; SVZ: Sestri Voltaggio zone; IL Insubric line. Modified from Bigi et al., (1990).

B) Schematic cross section, flattened at the base of the Pliocene, showing the relationships among the Messinian units. PLG: Primary Lower Gypsum unit; RLG: Resedimented Lower Gypsum unit; SKB: Sturani key-bed; CRB: carbonate-rich beds. Not to scale. Numbers (1-4) indicate the position of the sections reported in Fig. 2: 1) Arnulfi; 2) Rio Berri; 3) Cascina Merlotti; 4) Pollenzo. Location in Panel A). From Dela Pierre et al., 2011.

Fig. 2:

Correlation scheme of the studied sections (the trace is reported in Fig. 1A). Datum plane: base of the Sturani key-bed. The number and position of the laminated layers is indicated by green (peloidal layers) and red (filament-bearing layers) lines. SAF: Sant'Agata Fossili Marls; RLG: Resedimented Lower Gypsum; MES: Messinian erosional surface. PLG 1-PLG 13: Primary Lower Gypsum cycles. The Arnulfi section (not described) is also reported for correlation purposes. Modified from Dela Pierre et al., (2011).

Fig. 3:

A) The Rio Berri section. Numbers on the left indicate the laminated layers. The studied samples (BE 1-BE 9) and the corresponding stable isotope values are shown. A semi-quantitative estimate of the abundance of planktic foraminifers in the studied thin sections is reported as number of specimens/$cm^2$; f: frequent (>3/$cm^2$); c: common (1-3/$cm^2$); r: rare (<1/$cm^2$).

B) Outcrop view of the section, showing the position of the laminated layers (1-9).

Fig. 4: Rio Berri section.

A) Outcrop view of the lower part of the section: the alternation of terrigenous bedsets and cemented layers (4, 5 and 6) is clearly visible.

B) Outcrop view of the unconsolidated layers 7, 8 and 9. Two sandstone beds are visible below layers 7 and 9.

C) Close up of the cemented layer 6: arrows indicate the whitish packets interbedded to brownish terrigenous laminae; the base of a sandy layer can be seen at its top.

D) Close up of the unconsolidated layer 9. The laminated structure is clearly recognizable.

E) Polished slab, cut perpendicular to the bedding of sample BE2. Grey graded terrigenous laminae alternated with whitish composite packets are clearly recognizable. In these packets sub-mm thick dolomite-rich laminae alternate with dark mud-rich ones. The white arrow indicates the slightly erosional base of a silty lamina.

F) Polished slab cut perpendicular to the bedding of sample BE6. The structure is similar to that of Fig. 4E, except for the more wrinkled lamination of whitish dolomite-rich packets. The white arrows indicate the erosional base of two silty laminae.



Fig. 5: Peloidal layers.

Polished slab cut parallel to the bedding of sample BE1. Arrows point to the three types of peloids (type1, 2 and 3) described in the text.

B) Photomicrograph of a faecal pellet (type 1 peloid). Note the regular circular outline, the sharp boundary and the composite structure. Sample BE1.

C), D): photomicrographs in transmitted and UV light of sample BE 3. Note in C) the irregular boundaries of both type 2 and 3 peloids, the composite structure of type 2 peloids and the homogeneous composition of type 3 ones. In D) note the brighter autofluorescence of type 2 peloids compared to that of type 3 ones.

E), F): photomicrographs in transmitted and UV light of sample BE 3, showing type 1 and type 3 peloids. In F) note the brighter autofluorescence of type 1 peloids compared to that of type 3 ones.

Fig. 6: Selected Raman spectra of dolomicrosparite (sample BE2) and of dark filaments (sample BE5). Numbers in bold indicate peaks related to marcasite, those in italic the possibly peaks of pyrite; the others indicate dolomite peaks .

Fig. 7. Peloidal layers.

A) Photomicrograph of an isolated diatom mold, partially filled with dolomite microcrystals; Sample BE3.

B) Planktic foraminifer test; sample BE1.

C) SEM image of a cluster of molds of elongated diatoms; sample BE2.

D) SEM image of the imprint left by a *Surirella* sp. frustule sample BE3.

E) detail of the mold of elongated diatoms; sample BE2

F): mold of a centric diatom (*Coscinodiscus sp.)*. The arrow indicates isoriented dolomite microcrystals growing through the original frustule; sample BE1

G) Polished slab of sample BE2, cut slightly oblique to the bedding; top to the left. Most laminae (a) are made up of a mixture of type 2 and 3 peloids with sparse molds of centric diatoms, planktic foraminifers and land plant debris. Type 1 peloids (faecal pellets, arrow) are concentrated in distinctive laminae. Dark lamina on the left (b) is faintly graded and made up of silt grains and carbonaceous fragments. Scattered silt grains are also present in lamina c), made up of smaller type 2 peloids.

Fig. 8. Filament-bearing layers.

A) Polished slab, cut parallel to the bedding, of sample BE5. Note the maze of white filaments; some filaments are dark-coloured (black arrows) because of the presence of iron sulphide inclusions. The white arrow indicate a possible peloid.

B) Close up of whitish filaments in unconsolidated layer 9. Sample BE9.

C) Polished slab, cut slightly oblique to the bedding, of sample BE5 showing the contact between a terrigenous lamina below and a filament-bearing one above. Note that some filaments penetrate down into the topmost part of the terrigenous lamina (black arrows).

D) , E): photomicrographs in transmitted and UV light of sample BE6. Curved filaments with a bright autofluorescence are recognisable.

F) SEM backscatter image of sample PG1 (Pollenzo section, cycle PLG 4): arrows indicate filaments containing bright iron sulphide grains that are also dispersed in the matrix.

Fig. 9:

A) Close up of the mudstone interval below cycle PLG4: two laminated layers (white arrows) can be recognised. Cascina Merlotti section.

B) The mudstone interval below the Sturani-key bed (SKB), corresponding the the 6$^{th}$ PLG cycle. Cascina Merlotti section. Hammer for scale.

C) Close up of B): a laminated layer is clearly recognisable.

Fig. 10:

Sketch showing the depositional and early diagenetic processes giving origin to peloidal and filament-bearing layers.

A) Peloidal layers (see Fig. 4E); a flocculent layer deposited on an anoxic sea bottom was the site of dolomite precipitation in the very shallow subsurface via bacterial sulphate reduction (BSR). Early precipitation of dolomite was responsible for preservation of the delicate peloidal structure.

B) Filament-bearing layers (see Fig. 4F); a flocculent layer deposited on a slightly oxygenated sea bottom was colonized by sulphide-oxidizing *Beggiatoa*-like prokaryotes sustained by hydrogen sulphide fluxes sourced by bacterial sulphate reduction (BSR) from below. Dolomite precipitation via bacterial sulphate reduction (BSR) could take place only in buried bacterial mats, whereas bacterial sulphide oxidation (BSO) was active in the living chemotrophic mat.

In both sketches yellow arrows indicate the supply of Ca ions from dissolution of calcite skeletal remains. For further explanation, see text.

Fig. 11:

Facies stacking pattern in the muddy hemicycles and supposed short-term (sub-Milankovithcian) climate oscillations; blue line: insolation curve; black curve: higher frequency (plurisecular to millennary?) oscillations; red line (inset): annual to pluriannual (?) oscillations, recorded only in the laminated layers. The transition from peloidal- to filament-rich layers indicate a change from less to more oxygenated conditions at the sediment/water interface For further explanation, see text.

Table 1. Mineralogical composition, inferred through XRPD, of the peloid- and filament-bearing layers of the Rio Berri and Pollenzo sections (data expressed as wt%, standard deviations indicated in brackets).

Table 2 Stable isotope data of the Rio Berri layers

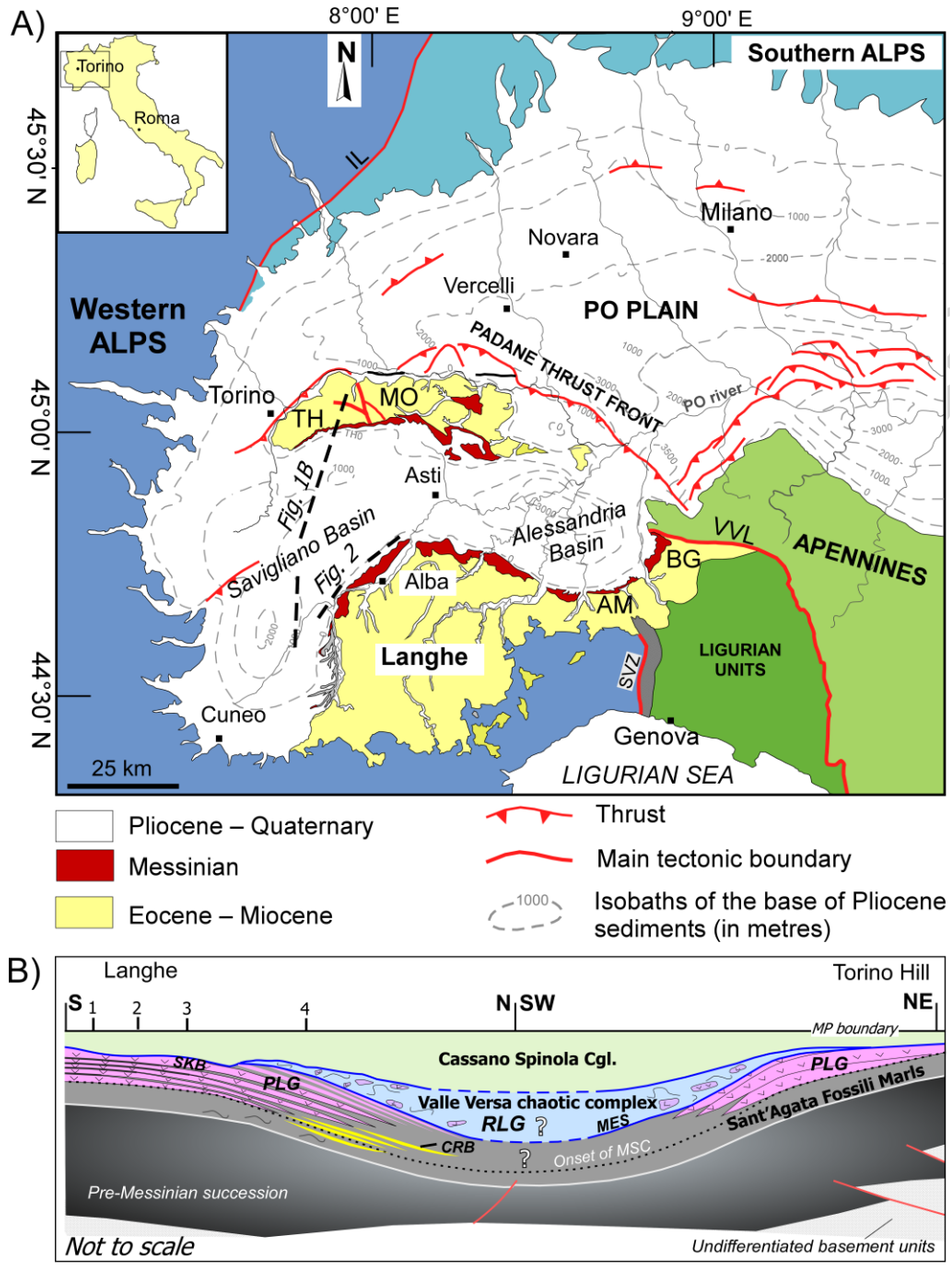


Dela Pierre et al., Fig. 1

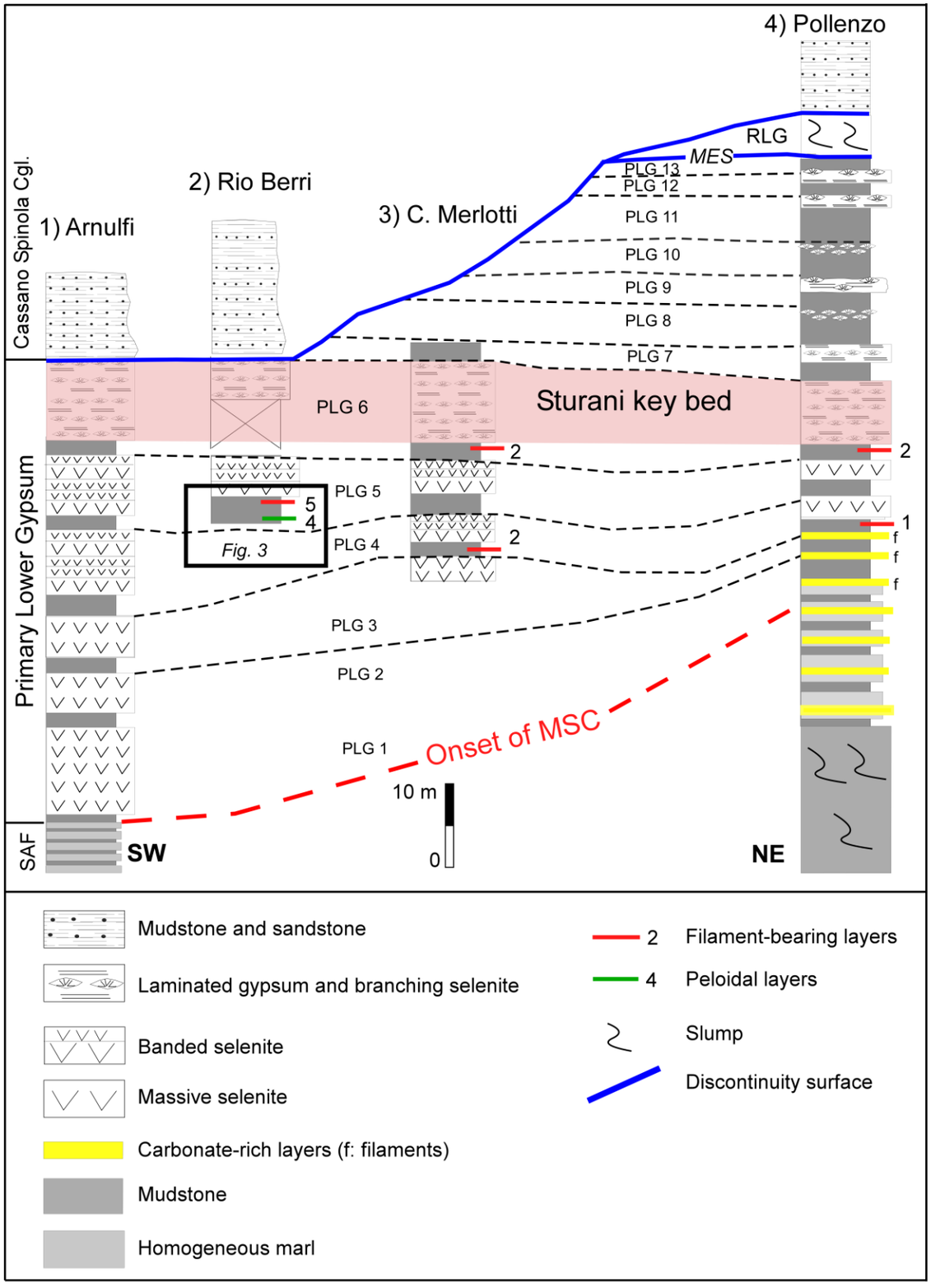


Dela Pierre et al., Fig. 2

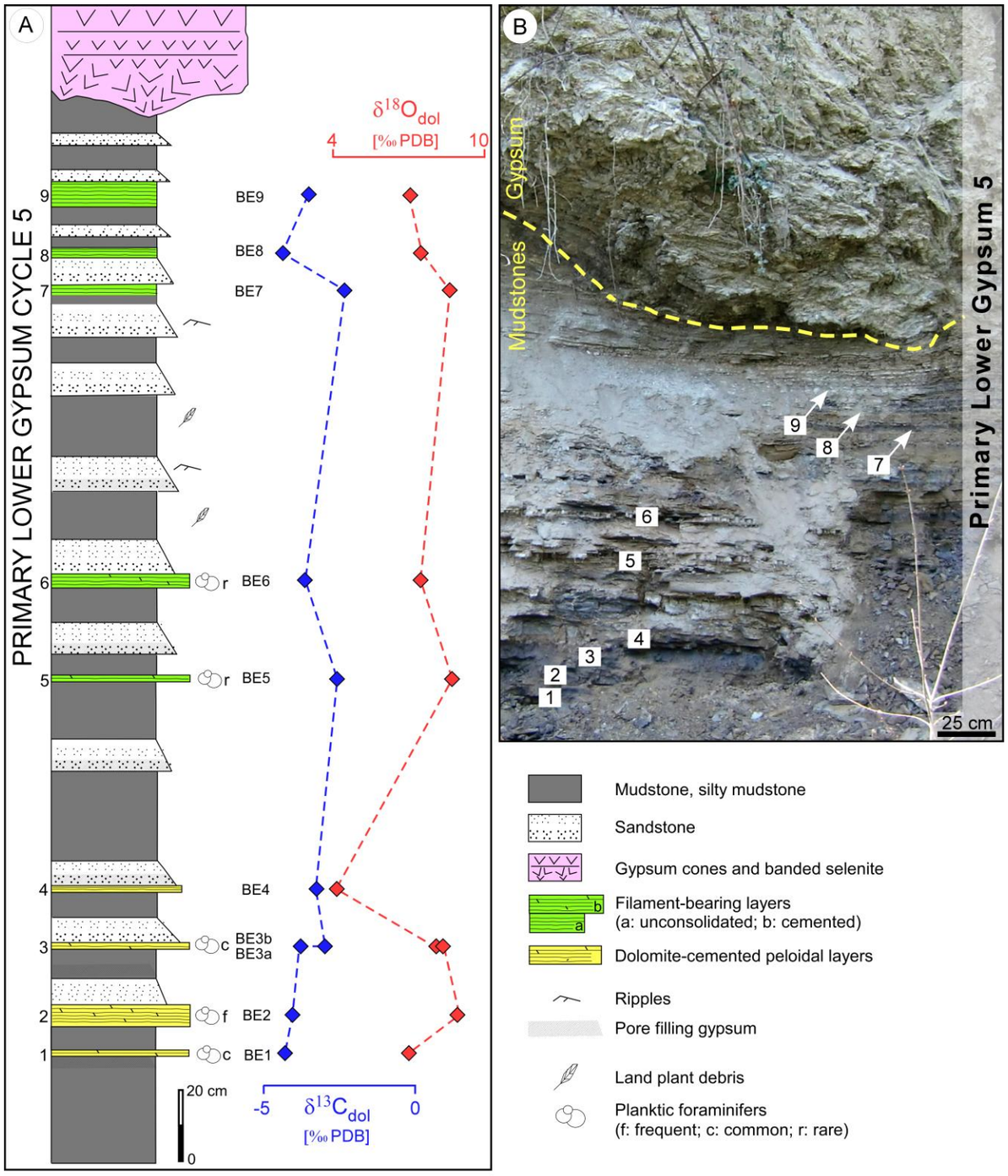


Dela Pierre et al., Fig. 3

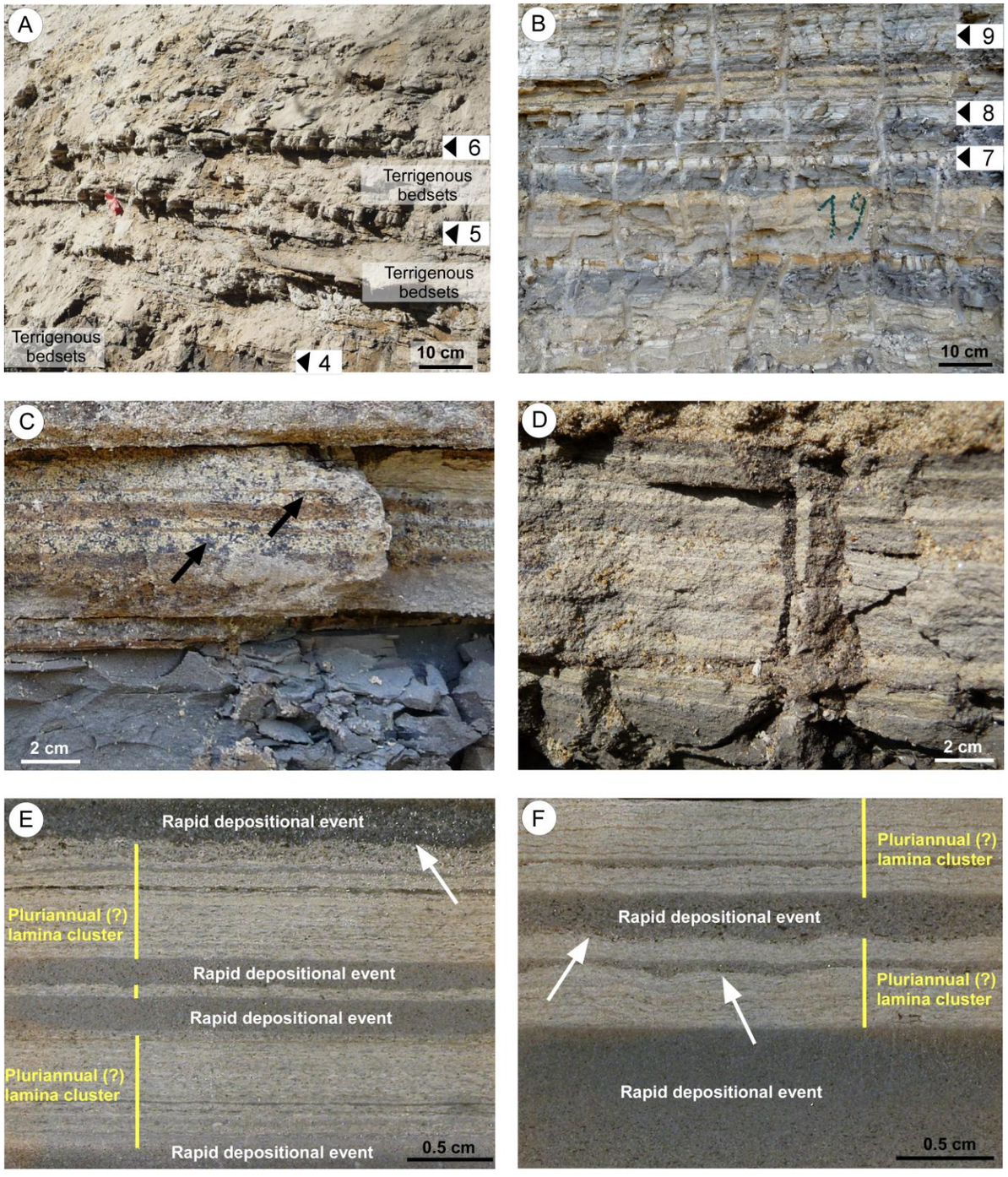


Dela Pierre et al Fig. 4

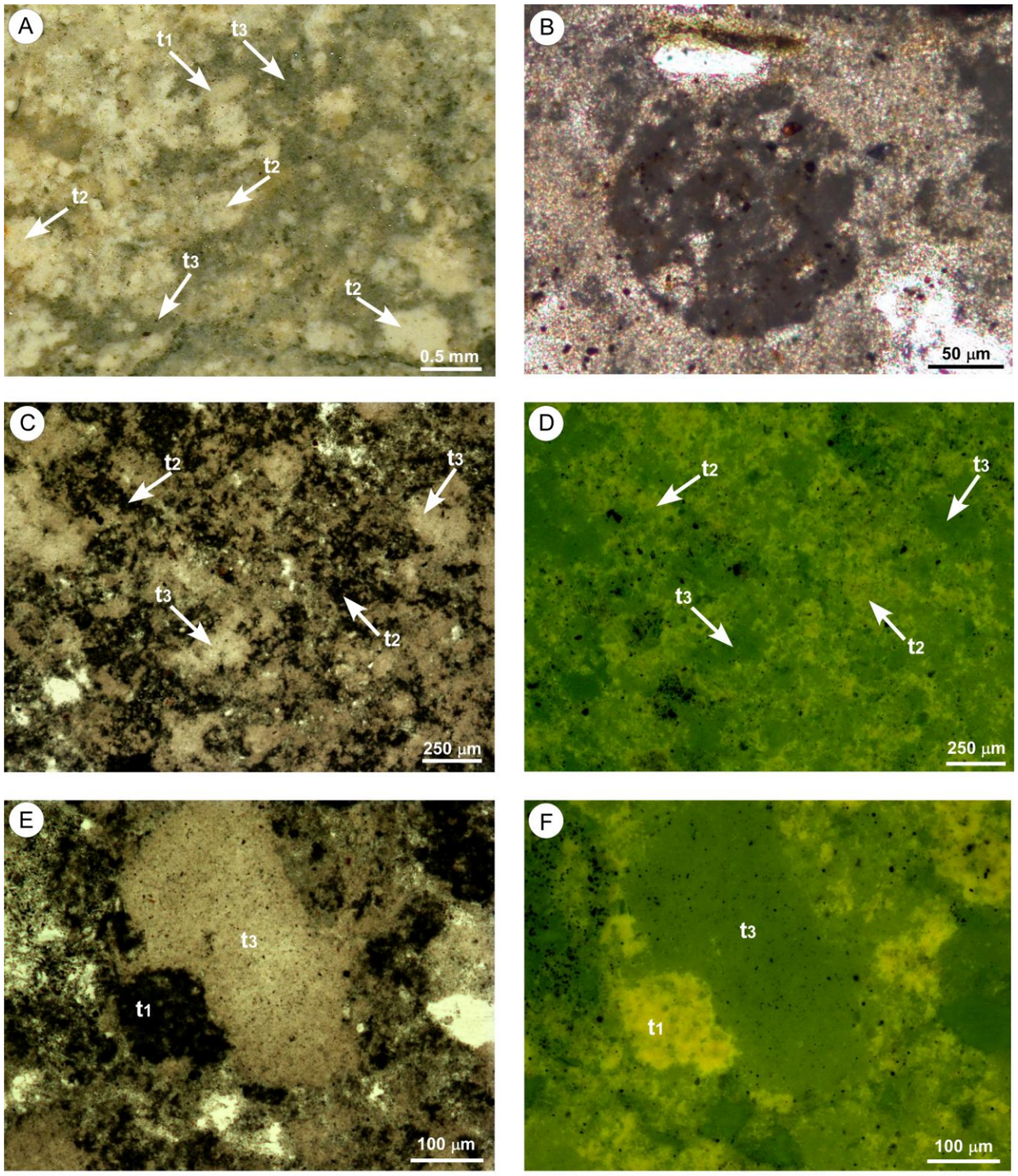


Dela Pierre et al., Fig. 5

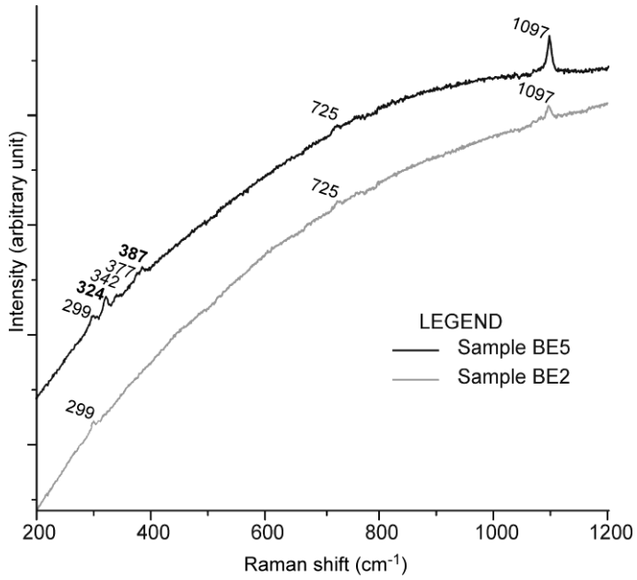


Dela Pierre et al. Fig. 6

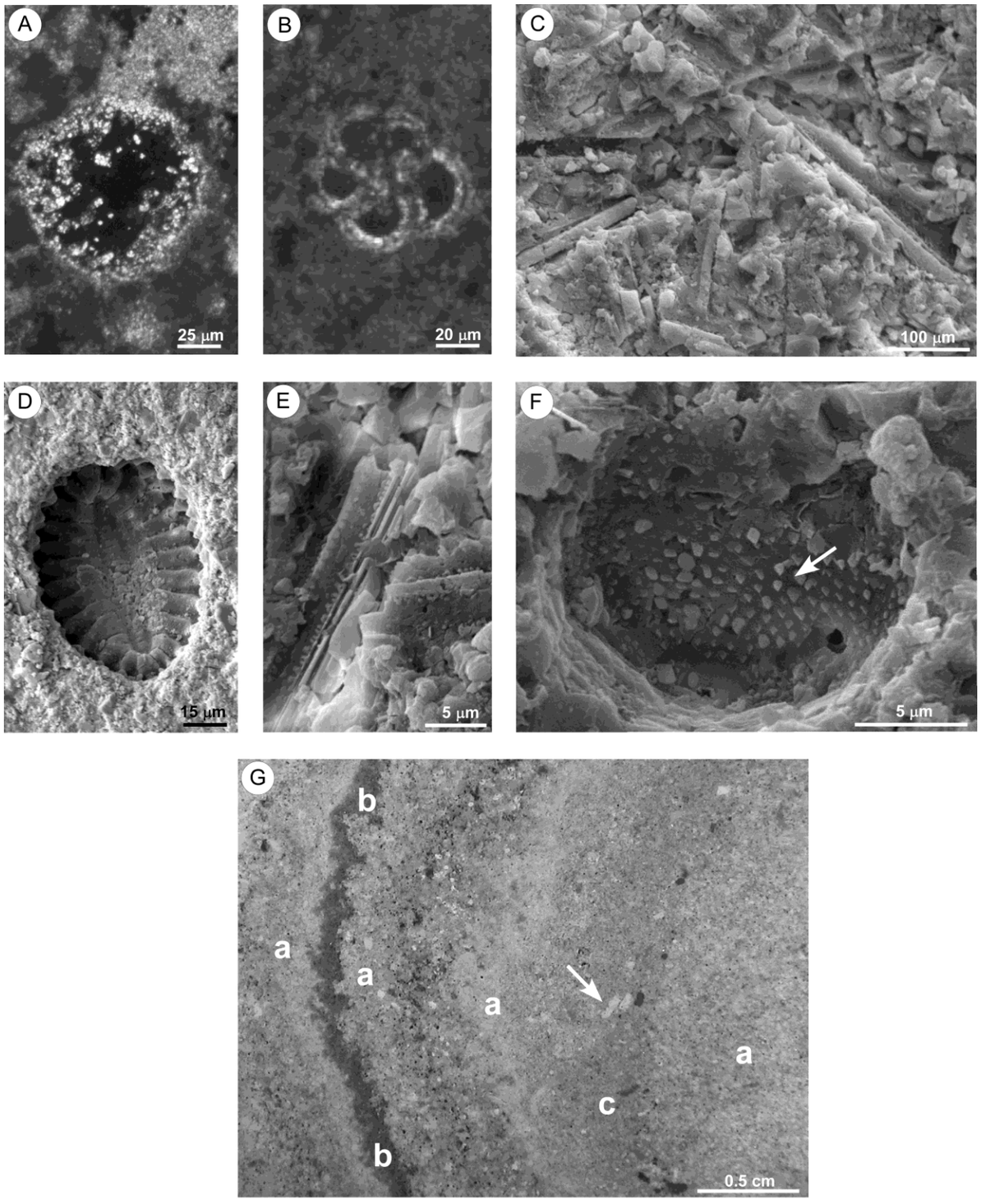


Dela Pierre et al., Fig. 7

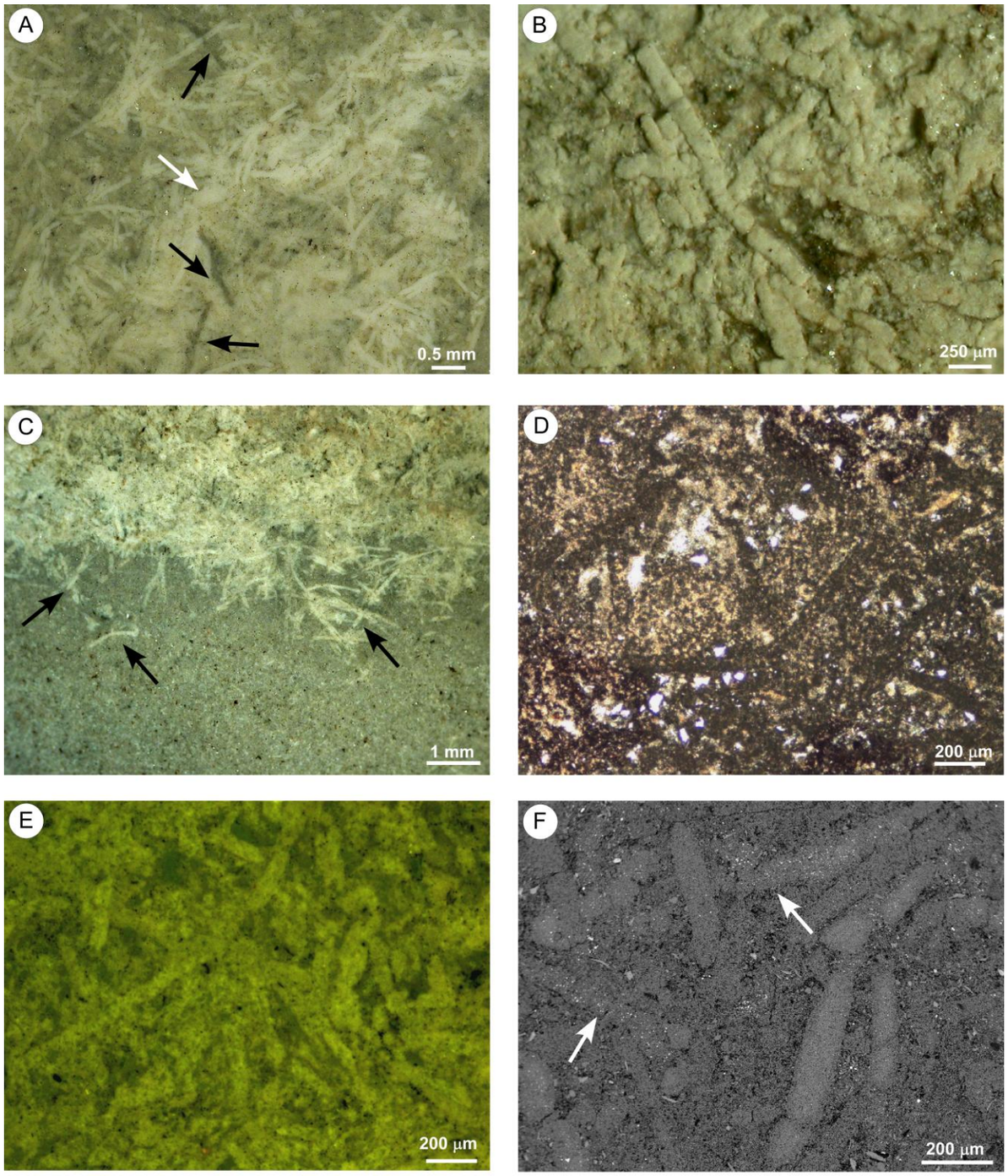


Dela Pierre et al., Fig. 8

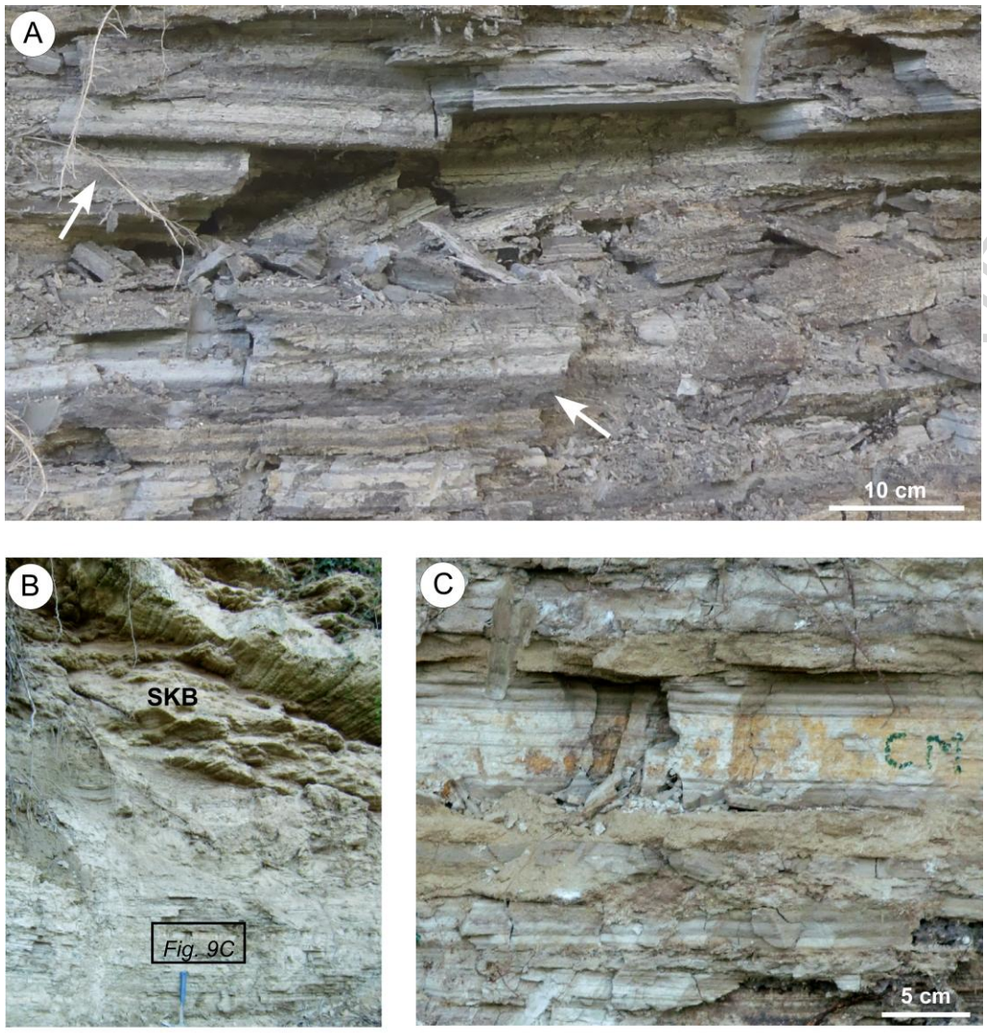


Dela Pierre et al., Fig. 9

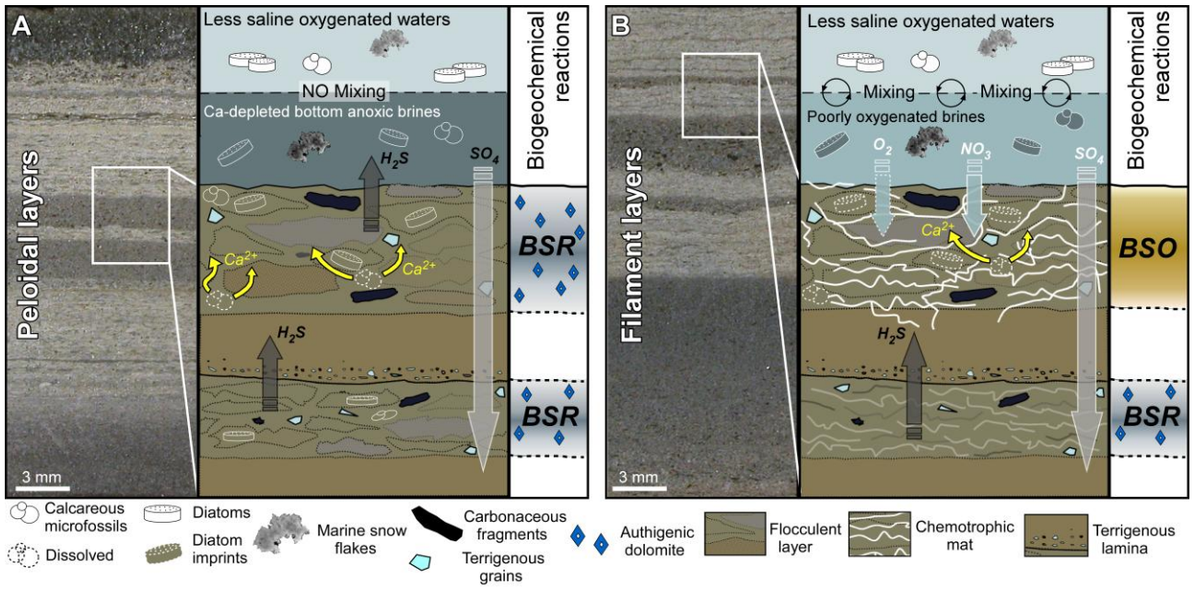


Dela Pierre et al., Fig. 10

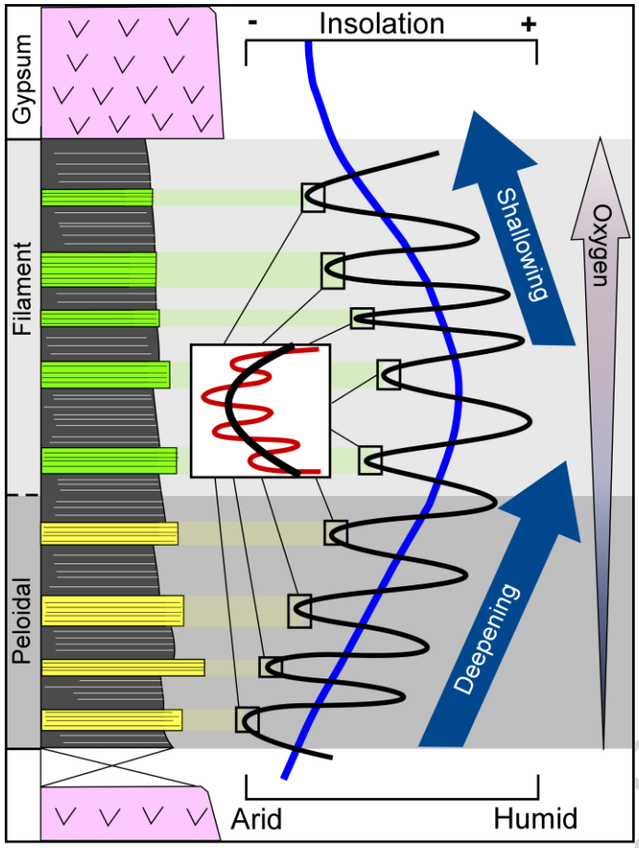


Dela Pierre et al. FIG. 11

| | Rio Berri section | | | | | | | | | | | Pollenzo section | | |
|---|---|---|---|---|---|---|---|---|---|---|---|---|---|---|
| | Peloid-bearing layers | | | | | Filament-bearing layers | | | | | | Filament bearing layers | | |
| | Samples | | | | | | | | | | | Samples | | |
| | **BE1** | **BE2** | **BE3** | **BE4** | **Average** | **BE5** | **BE6** | **BE7** | **BE8** | **BE9** | **Average** | **PG1** | **PG3.1** | **Average** |
| **Mineral** | | | | | | | | | | | | | | |
| Dolomite | 55.9(2) | 73.5(1) | 67.4(2) | 11.4(4) | 52.1 wt% | 61.7(2) | 68.5(1) | 47.7(3) | 46.4(3) | 36.5(3) | 52.2 wt% | 39.0(3) | 45.4(3) | 42.2 wt% |
| Quartz | 10.6(2) | 5.0(2) | 10.2(2) | 27.5(2) | 13.3 wt% | 11.0(4) | 6.9(2) | 12.4(3) | 12.9(2) | 23.8(2) | 13.4 wt% | 7.0(2) | 7.7(2) | 7.4 wt% |
| Clinochlore | 4.1(4) | 2.6(4) | 3.1(3) | 6.2(7) | 4.0 wt% | 4.1(4) | 3.0(4) | 3.2(5) | 7.1(6) | 3.7(4) | 4.2 wt% | 9.0(9) | 4.1(4) | 6.6 wt% |
| Kaolinite | 4.4(3) | 2.7(3) | 2.6(3) | 3.3(3) | 3.3 wt% | 4.0(3) | 4.7(5) | 6.5(3) | 5.6(4) | 8.9(5) | 5.9 wt% | 4.0(3) | 10.9(5) | 7.5 wt% |
| Illite | 2.4(2) | 3.6(6) | 6.7(4) | 4.7(4) | 4.3 wt% | 4.4(3) | 2.4(2) | 4.7(4) | 5.5(3) | = | 3.4 wt% | 11.4(6) | 3.2(3) | 7.3 wt% |
| (Clay fraction) | 10.9 | 8.9 | 12.4 | 14.2 | 11.6 wt% | 12.5 | 10.1 | 14.4 | 18.2 | 12.6 | 13.5 wt% | 24.4 | 18.2 | 21.4 wt% |
| Muscovite | 13.2(4) | 6.8(5) | 6.2(5) | 29.8(5) | 14.0 wt% | 10.9(5) | 7.9(5) | 15.8(6) | 15.2(6) | 22.0(8) | 14.4 wt% | 15.7(5) | 16.0(6) | 15.8 wt% |
| Albite | 4.8(4) | 4.7(4) | 3.2(2) | 10.0(8) | 5.7 wt% | 3.5(3) | 3.7(3) | 3.0(3) | 5.9(4) | 2.8(3) | 3.8 wt% | 12(1) | 4.0(4) | 8.0 wt% |
| Anorthite | 2.0(2) | 1(1) | 0.5(8) | 5.6(5) | 2.3 wt% | 0.4(2) | 1.1(2) | 6.0(4) | 1.2(1) | 2.3(2) | 2.2 wt% | 1.5(2) | 8.7(6) | 5.1 wt% |
| (Plagioclase) | 6.8 | 5.7 | 3.7 | 15.6 | 8.0 wt% | 3.9 | 4.8 | 9.0 | 7.1 | 5.1 | 6.0 wt% | 13.5 | 12.7 | 13.1 wt% |
| Gypsum | 2.4(2) | = | = | 1.5(2) | 0.9 wt% | = | 1.7(1) | 0.8(9) | 0.2(9) | = | 0.5 wt% | = | = | = |
| **Total** | 99.8 | 99.9 | 99.9 | 100.0 | 99.9 wt% | 100.0 | 99.9 | 100.1 | 100.0 | 100.0 | 100.0 wt% | 99.6 | 100.0 | 99.9 wt% |

**Clari et al., Table 1.**

| Sample | Type of layer | $\delta^{13}C_{dol}$ [‰] | $\delta^{18}O_{dol}$ [‰] |
|---|---|---|---|
| BE1 | Peloidal | −4.2 | +7.0 |
| BE2 | Peloidal | −3.9 | +8.9 |
| BE3a | Peloidal | −3.5 | +8.1 |
| BE3b | Peloidal | −2.6 | +8.3 |
| BE4 | Peloidal | −2.9 | +4.1 |
| BE5 | Filament-bearing | −2.1 | +8.7 |
| BE6 | Filament-bearing | −3.3 | +7.5 |
| BE7 | Filament-bearing | −1.8 | +8.6 |
| BE8 | Filament-bearing | −4.2 | +7.4 |
| BE9 | Filament-bearing | − 3.2 | +7.1 |

Clari et al., Table 2

Highlights

1) Laminated beds were identified in the mudstone of the Primary Lower Gypsum unit

2) They correspond to Messinian flocculent layers and chemotrophic microbial mats

3) Preservation results from complex biogeochemical reactions during the salinity crisis

4) These beds record short term climate changes at insolation maxima

5) Their stacking pattern records improved bottom oxygenation